

## Supporting Information

to

# Effect of conformational flexibility on photophysics of bis-coumarins.

*Łukasz Kielesiński,<sup>a,b</sup> Daniel T. Gryko<sup>a,\*</sup> Andrzej L. Sobolewski<sup>b,\*</sup> and Olaf W. Morawski,<sup>b,\*</sup>*

*<sup>a</sup>Institute of Organic Chemistry, Polish Academy of Sciences, Kasprzaka 44/52, 01-224  
Warsaw, Poland.*

*<sup>b</sup>Institute of Physics, Polish Academy of Sciences, Al. Lotników 32/46, 02-668 Warsaw,  
Poland.*

### Table of Contents

1. General Information	2
2. Synthesis	2
3. Theoretical methods	4
4. Experimental methods	5
5. Computational results	6
6. Photophysical measurements results	27
7. IR and Raman spectra	34
8. Copies of NMR spectra	37

## 1. General information.

Dichloroethane, tetrahydrofuran and dimethylformamide were dried over phosphorus pentoxide, sodium and potassium alloy and magnesium sulfate respectively prior to use. All reported NMR spectra ( $^1\text{H}$  NMR and  $^{13}\text{C}$  NMR) were recorded using a Varian 500 and 600 spectrometer. Chemical shifts ( $\delta$  ppm) were determined with TMS as the internal reference,  $J$  values are given in Hz. High resolution mass spectra (HRMS) were obtained via electron ionization (EI) and electrospray ionization (ESI). IR spectra were recorded on JASCO FT/IR-6200 Spectrometer. UV-Vis absorption spectra were recorded on PerkinElmer Lambda 35 Spectrometer. Fluorescence spectra were recorded on Fluorolog TCSPC Horiba. Fluorescence lifetimes were measured on Laser Mira Coherent. Chromatography was performed on silica gel 60 (230-400 mesh) and thin layer chromatography was performed on TLC plates (Merck, silica gel 60 F<sub>254</sub>).

## 2. Synthesis.

### Typical procedure for the synthesis of aminocoumarins.

To the solution of nitrocoumarin (0.5 mmol) in ethanol tin dichloride dihydrate (2 mmol) was added. The reaction mixture was refluxed for 2 hours. Then the mixture was cooled to room temperature and aqueous  $\text{NaHCO}_3$  was added until the pH was neutral. The aqueous solution was extracted with AcOEt and the combined organic layers were dried over  $\text{Na}_2\text{SO}_4$  and concentrated under reduced pressure. The crude product was crystallized from AcOEt-cyclohexane affording product of analytical purity.

#### Ethyl 7-amino-2-oxo-2H-chromene-3-carboxylate (3)

Yellow precipitate, 0.114g, 97% yield. M.p. 228-229 °C.  $^1\text{H}$  NMR ( $\text{CDCl}_3$ , 500 MHz):  $\delta$  8.44 (s, 1H, CH), 7.36 (d,  $J$  = 8.2 Hz, 1H, Ar), 6.56 (s, 2H, Ar), 4.54 (bs, 2H,  $\text{NH}_2$ ), 4.38 (q,  $J$  = 7.1 Hz, 2H,  $\text{OCH}_2\text{CH}_3$ ), 1.39 (t,  $J$  = 7.0 Hz, 3H,  $\text{OCH}_2\text{CH}_3$ ).  $^{13}\text{C}$  NMR ( $\text{CDCl}_3$ , 125 MHz):  $\delta$  14.3, 61.4, 99.9, 109.7, 111.3, 112.6, 131.4, 149.4, 153.3, 157.9, 158.2, 164.6. HRMS (ESI-TOF):  $m/z$  calculated for  $\text{C}_{12}\text{H}_{11}\text{NO}_4$  [ $\text{M}^+\text{Na}$ ] $^+$  = 256.0580; found: 256.0586.

#### Ethyl 6-amino-2-oxo-2H-chromene-3-carboxylate (11)

Yellow precipitate, 0.228g, 98% yield. M.p. 158-160 °C.  $^1\text{H}$  NMR ( $\text{CDCl}_3$ , 500 MHz):  $\delta$  8.38 (s, 1H, CH), 7.16 (d,  $J$  = 8.8 Hz, 1H, Ar), 6.98 (dd,  $J$  = 8.8, 2.8 Hz, 1H, Ar), 6.81 (d,  $J$  = 2.8 Hz, 1H, Ar), 4.40 (q,  $J$  = 7.2 Hz, 2H,  $\text{OCH}_2\text{CH}_3$ ), 3.80 (bs, 2H,  $\text{NH}_2$ ), 1.40 (t,  $J$  = 7.2 Hz, 3H,  $\text{OCH}_2\text{CH}_3$ ).  $^{13}\text{C}$  NMR ( $\text{CDCl}_3$ , 125 MHz):  $\delta$  14.2, 61.9, 112.4, 117.5, 118.3, 118.4, 122.4, 143.4, 148.3, 148.5, 157.2, 163.4. IR (KBr,  $\text{cm}^{-1}$ ): 796, 1038, 1133, 1242, 1380, 1571, 1750, 2982, 3059, 3223, 3330, 3404. HRMS (EI):  $m/z$  calculated for  $\text{C}_{12}\text{H}_{11}\text{NO}_4$  [ $\text{M}^+$ ] = 233.0688; found: 233.0686.

### The synthesis of Amide-7

The 7-(diethylamino)-2-oxo-2H-chromene-3-carboxylic acid (0.3 mmol), T<sub>3</sub>P in DCM (0.36 mmol) and dry DCE were placed in dry Schlenk tube flask under argon. DIPEA (0.33 mmol) was subsequently added and the reaction mixture was stirred at room temperature. Then the ethyl 7-amino-2-oxo-2H-chromene-3-carboxylate (0.36 mmol) was added and the mixture was refluxed overnight. The reaction mixture was cooled to room temperature, diluted with water and extracted with DCM. The combined organic layers were dried over  $\text{Na}_2\text{SO}_4$  and concentrated under reduced pressure. The crude product was purified by column

chromatography (silica, DCM/MeOH 95:5). Crystallization from AcOEt-cyclohexane afforded product of analytical purity.

#### Amide-7

Yellow precipitate, 0.030g, 21% yield. M.p. 289-291 °C. <sup>1</sup>H NMR (CDCl<sub>3</sub>, 600 MHz): δ 11.33 (s, 1H, NH), 8.80 (s, 1H, CH), 8.49 (s, 1H, CH), 8.07 (s, 1H, Ar), 7.54-7.57 (m, 1H, Ar), 7.47-7.53 (m, 2H, Ar), 6.70 (dd, *J* = 12.0, 6.0 Hz, 1H, Ar), 6.54 (s, 1H, Ar), 4.41 (q, *J* = 6.0 Hz, 2H, OCH<sub>2</sub>CH<sub>3</sub>), 3.49 (q, *J* = 6.0 Hz, 4H, NCH<sub>2</sub>CH<sub>3</sub>), 1.41 (t, *J* = 6.0 Hz, 3H, OCH<sub>2</sub>CH<sub>3</sub>), 1.27 (t, *J* = 6.0 Hz, 6H, NCH<sub>2</sub>CH<sub>3</sub>). Due to the very low solubility we could not register the <sup>13</sup>C NMR spectrum. HRMS (EI): *m/z* calculated for C<sub>26</sub>H<sub>24</sub>N<sub>2</sub>O<sub>7</sub> [M<sup>+</sup>] = 476.1584; found: 476.1581.

#### The synthesis of Ester-7

To the solution of 7-(diethylamino)-2-oxo-2*H*-chromene-3-carboxylic acid (0.4 mmol) in dry DCE, ethyl 7-hydroxy-2-oxo-2*H*-chromene-3-carboxylate (0.4 mmol), EDC (0.6 mmol) and DMAP (0.2 mmol) were added. The reaction mixture was stirred under argon overnight. The mixture was diluted with water and extracted with DCM. The combined organic layers were dried over Na<sub>2</sub>SO<sub>4</sub> and concentrated under reduced pressure. The crude product was crystallized from DCM-cyclohexane affording product of analytical purity.

#### Ester-7

Yellow precipitate, 0.048g, 25% yield. M.p. 198-200 °C. <sup>1</sup>H NMR (CDCl<sub>3</sub>, 500 MHz): δ 8.61 (s, 1H, CH), 8.53 (s, 1H, CH), 7.64 (d, *J* = 8.3 Hz, 1H, Ar), 7.43 (d, *J* = 8.9 Hz, 1H, Ar), 7.25-7.29 (m, 2H, Ar), 6.68 (dd, *J* = 9.1, 2.4 Hz, 1H, Ar), 6.52 (d, *J* = 2.0 Hz, 1H, Ar), 4.42 (q, *J* = 7.1 Hz, 2H, OCH<sub>2</sub>CH<sub>3</sub>), 3.49 (q, *J* = 7.1 Hz, 4H, NCH<sub>2</sub>CH<sub>3</sub>), 1.42 (t, *J* = 7.1 Hz, 3H, OCH<sub>2</sub>CH<sub>3</sub>), 1.27 (t, *J* = 7.1 Hz, 6H, NCH<sub>2</sub>CH<sub>3</sub>). <sup>13</sup>C NMR (CDCl<sub>3</sub>, 125 MHz): δ 12.4, 14.2, 45.4, 62.0, 96.9, 106.4, 108.0, 110.2, 110.5, 115.6, 117.4, 119.4, 130.2, 131.7, 148.1, 150.7, 153.6, 155.6, 156.0, 156.4, 157.8, 159.0, 161.8, 163.0. IR (KBr, cm<sup>-1</sup>): 1194, 1346, 1508, 1581, 1618, 1766, 2978, 3056. HRMS (EI): *m/z* calculated for C<sub>26</sub>H<sub>23</sub>NO<sub>8</sub> [M<sup>+</sup>] = 477.1424; found: 477.1440. Elemental analysis (%): calculated for C<sub>26</sub>H<sub>23</sub>NO<sub>8</sub>: C, 65.40; H, 4.86; N, 2.93; found: C, 65.28; H, 4.75; N, 3.09.

#### The synthesis of Amide-6

To the solution of 7-(diethylamino)-2-oxo-2*H*-chromene-3-carboxylic acid (0.5 mmol) in dry DCE, ethyl 6-amino-2-oxo-2*H*-chromene-3-carboxylate (0.5 mmol), EDC (0.6 mmol) and DMAP (cat. amount) were added. The reaction mixture was stirred under argon overnight. The mixture was diluted with water and extracted with DCM. The combined organic layers were dried over Na<sub>2</sub>SO<sub>4</sub> and concentrated under reduced pressure. The crude product was crystallized from DCM-cyclohexane affording product of analytical purity.

#### Amide-6

Yellow precipitate, 0.165g, 69% yield. M.p. 272-274 °C. <sup>1</sup>H NMR (CDCl<sub>3</sub>, 500 MHz): δ 11.09 (s, 1H, NH), 8.77 (s, 1H, CH), 8.53 (s, 1H, CH), 8.29 (d, *J* = 2.7 Hz, 1H, Ar), 7.78 (dd, *J* = 8.9, 2.7 Hz, 1H, Ar), 7.48 (d, *J* = 8.9 Hz, 1H, Ar), 7.33 (d, *J* = 8.9 Hz, 1H, Ar), 6.71 (dd, *J* = 8.9, 2.4 Hz, 1H, Ar), 6.55 (d, *J* = 2.4 Hz, 1H, Ar), 4.42 (q, *J* = 7.2 Hz, 2H, OCH<sub>2</sub>CH<sub>3</sub>), 3.49 (q, *J* = 7.2 Hz, 4H, NCH<sub>2</sub>CH<sub>3</sub>), 1.42 (t, *J* = 7.2 Hz, 3H, OCH<sub>2</sub>CH<sub>3</sub>), 1.27 (t, *J* = 7.2 Hz, 6H, NCH<sub>2</sub>CH<sub>3</sub>). <sup>13</sup>C NMR (CDCl<sub>3</sub>, 125 MHz): δ 12.4, 14.2, 45.3, 61.9, 96.8, 108.7, 109.4, 110.5, 117.1, 118.0, 118.6, 119.7, 126.7, 131.5, 135.3, 148.6, 148.7, 151.5, 153.0, 156.8, 157.8,

161.4, 163.0, 163.1. IR (KBr,  $\text{cm}^{-1}$ ): 788, 1020, 1186, 1258, 1511, 1552, 1610, 1692, 1748, 3047, 3201. HRMS (EI):  $m/z$  calculated for  $\text{C}_{26}\text{H}_{24}\text{N}_2\text{O}_7$  [ $\text{M}^+$ ] = 476.1584; found: 476.1592. Elemental analysis (%): calculated for  $\text{C}_{26}\text{H}_{24}\text{N}_2\text{O}_7$ : C, 65.54; H, 5.08; N, 5.88; found: C, 65.58; H, 5.05; N, 5.92.

### 3. Theoretical methods

The ground-state equilibrium geometry of investigated molecular systems was determined with the second-order Møller-Plesset (MP2) method. Excitation energies, excited-state reaction paths and energy profiles were calculated with the second-order algebraic-diagrammatic-construction (ADC(2)) method.<sup>1</sup> ADC(2) is a variant of propagator theory and is closely related to the approximate second-order singles-and-doubles coupled-cluster (CC2) method,<sup>2</sup> which is a widely used computationally efficient variant of coupled-cluster theory for excited states. The advantage of the ADC(2) method compared to the CC2 method is that the excitation energies are calculated as the eigenvalues of a Hermitian secular matrix. Moreover, the ADC(2) method is more stable in the vicinity of excited-state energy crossings and is able to describe the topography of conically intersecting potential-energy surfaces of excited states physically correctly.<sup>3</sup> Dunning's correlation-consistent split-valence double- $\zeta$  basis set with polarization functions on all atoms (cc-pVDZ)<sup>4</sup> was employed in the MP2 and ADC(2) calculations. In all considered molecular systems the terminal ethyl groups were replaced by methyl groups. This replacement has negligible effect on electronic properties of the system but significantly saves the computational time.

The reaction path for the excited-state intramolecular proton-transfer (ESIPT) process from the amide linker to the coumarin core as well as for the mutual twisting of the coumarin units was constructed at the ADC(2) level as a so-called relaxed scan, that is, for a fixed value of the driving coordinate (the NH distance involved in the hydrogen bonding and the CCNC dihedral angle, respectively) all other internal coordinates of the system were relaxed in the S1 electronic state. In these time-consuming computations a smaller def-SV(P) basis set was used.

The MP2 and ADC(2) calculations were carried out with the TURBOMOLE program package,<sup>5</sup> making use of the resolution-of-the-identity (RI) approximation<sup>6</sup> for the evaluation of the electron-repulsion integrals.

#### References for theoretical methods

- (1) Trovimon, A. B.; Schirmer, J. An Efficient Polarization Propagator Approach to Valence Excitation Spectra. *J. Phys. B: At. Mol. Opt. Phys.* **1995**, *28*, 2299-2324.
- (2) Christiansen, O.; Koch, H.; Jørgensen, P. The Second-Order Approximate Coupled Cluster Singles and Doubles Model CC2. *Chem. Phys. Lett.* **1995**, *243*, 409-418.
- (3) Köhn, A.; Tajti, A. Can Coupled-Cluster Theory Treat Conical Intersections? *J. Chem. Phys.* **2007**, *127*, 044105.
- (4) Dunning, Jr, T. H. Gaussian Basis Sets for Use in Correlated Molecular Calculations. I. The Atoms Boron Through Neon and Hydrogen. *J. Chem. Phys.* **1989**, *90*, 1007-1023.
- (5) TURBOMOLE, V6.3.1, **2011**. A Development of the University of Karlsruhe and Forschungszentrum Karlsruhe; available from <http://www.turbomole.com>.
- (6) Hättig, C.; Weigend, F. CC2 Excitation Energy Calculations on Large Molecules Using the Resolution of the Identity Approximation. *J. Chem. Phys.* **2000**, *113*, 5154-5161.

#### 4. Experimental methods

Spectroscopic grade solvents were purchased from Sigma-Aldrich and used as obtained. **Amide-6**, **Amide-7** and **Ester-7** are not soluble in n-alkanes but well soluble in polar and polarizable solvents. The initial solutions of concentrations about 80 micromoles per liter were diluted to the target 3  $\mu\text{M}$  used in optical studies. To exclude the presence of dimers the absorption and fluorescence spectra of initial concentrated solutions were compared with those of diluted solutions. Solutions of molecules in the solvents have been bubbled with pure Argon gas for 20 minutes before measurement.

All absorption and fluorescence spectra were taken at room temperature (21 $^{\circ}\text{C}$ ). Perkin Elmer UV/VIS Spectrometer model Lambda 35 was used for absorption spectra measurement. Fluorescence spectra were recorded with the aid of a Fluorolog-3 Spectrometer and corrected for the spectral response sensitivity of the photodetector.

Fluorescence quantum yields of biscoumarins in solvents at 21 $^{\circ}\text{C}$  were determined using perylene dissolved in cyclohexane ( $\Phi_{\text{F}} = 0.94$ ) as the standard. Solutions of low absorbance ( $A < 0.1$ ) were used to avoid reabsorption or concentration quenching. Corrections for refractive index of solvents have been performed in the calculations of quantum yields<sup>1</sup>.

Fluorescence kinetics studies were performed with the "time correlated" single photon counting technique. Fluorescence decays of **Amide-6** and **Amide-7** were excited with sub-ns pulses of Delta-Diode and recorded with Fluorolog-3 photomultiplier. For **Ester-7** excitation pulses (time-width  $\sim 30$  ps) were provided by the second harmonic of a mode-locked Coherent Mira-HP picosecond laser pumped by a Verdi 18 laser. Original repetition rate of a Mira laser was reduced with the aid of APE Pulse selector to 3.8 MHz. Fluorescence was dispersed with DK242T monochromator configured in subtractive dispersion mode. Fluorescence photons were detected with a HMP-100-50 hybrid detector and a SPC-150 module inserted into a PC, both from Becker&Hickl GmbH. Fluorescence decays were analyzed with a deconvolution computer program, which uses nonlinear least squares procedure with Marquardt method.<sup>2</sup> Standard  $\chi^2$  test was used along with residual and autocorrelation function plots to judge the quality of a fit. Estimated precision of the decay time determination was 10 ps.

#### References for experimental methods

- (1) Birks, J. B. *Photophysics of Aromatic Molecules*, Wiley, London, **1979**, pp. 97-100.
- (2) Demas, J. N. *Excited State Lifetime Measurements*, Academic Press, NY, **1983**, pp. 89-92.

## 5. Computational results

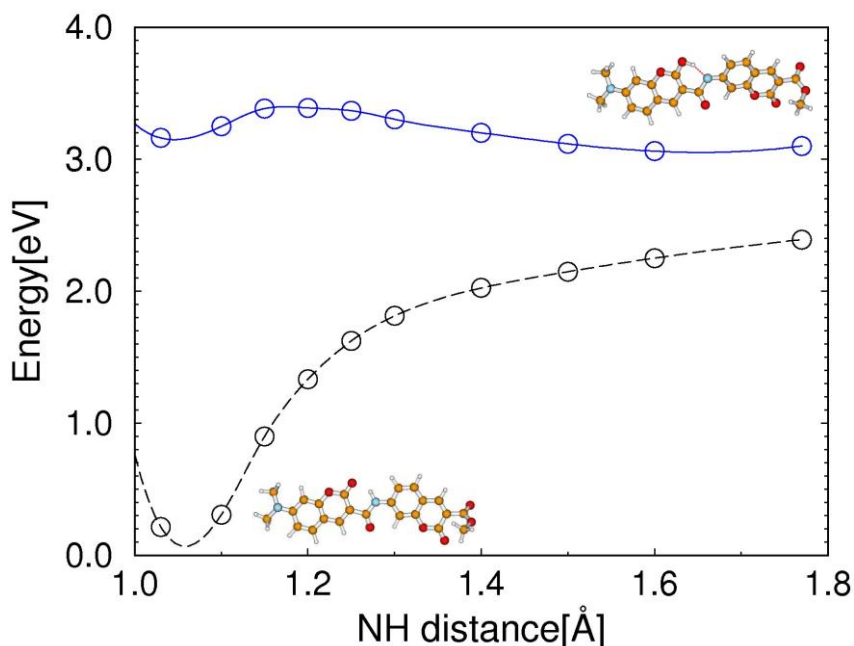


**Figure SF1.** Potential-energy (PE) profiles of the **Amide-7** computed at the MP2/ADC(2) level of theory along the proton-transfer (NH distance) coordinate. The solid line denotes the minimum-energy profile determined in the S<sub>1</sub> state while the dashed line represents the vertical-energy profile of the S<sub>0</sub> state computed at the optimized geometry of the S<sub>1</sub> state.

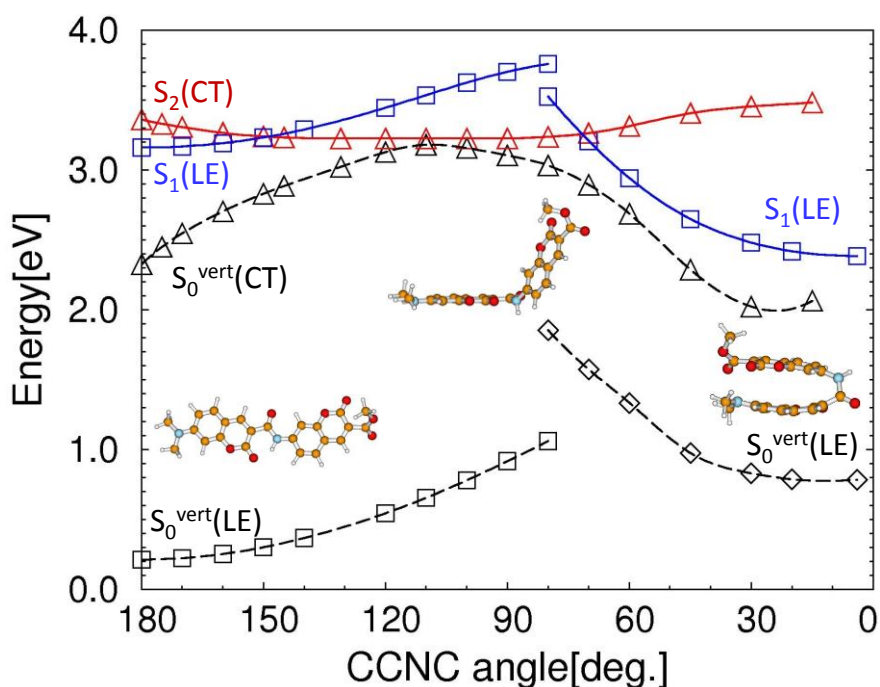


**Figure SF2.** Potential-energy (PE) profiles of the **Amide-7** computed at the MP2/ADC(2) level of theory along the amide group twisting (CCNC dihedral angle) coordinate. The solid lines denote the minimum-energy profile determined in excited states while the dashed line represents the vertical-energy profile of the S<sub>0</sub> state computed at the geometry of the respective excited state. The blue and the red lines denote potential-energy profile of the locally-excited and the charge-transfer state, respectively.

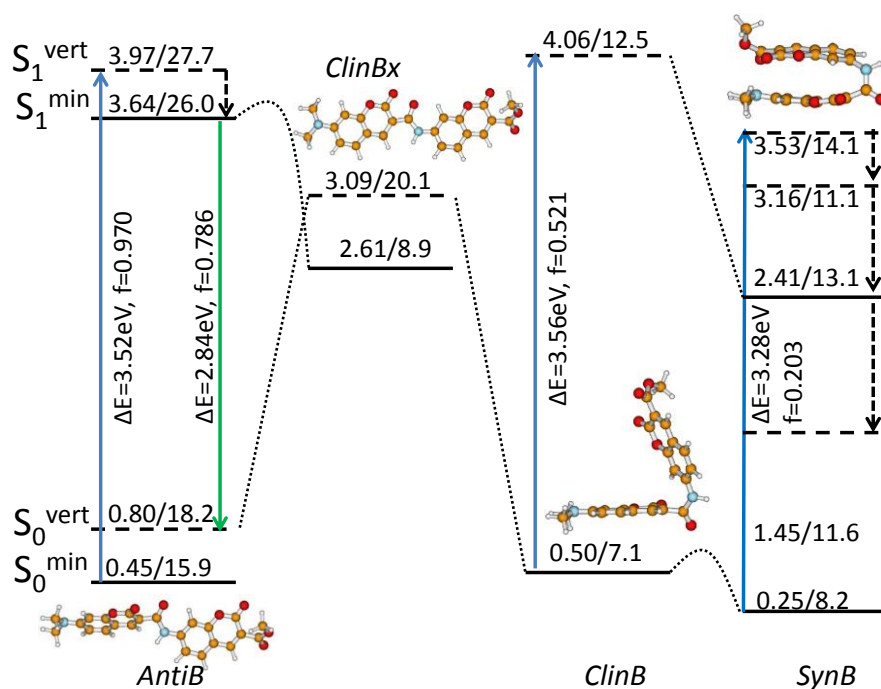


**Figure SF3.** Photophysical scheme of **Amide-7(B)** computed at the MP2/ADC(2) level of theory. Solid levels denote adiabatic (optimized) energy of a given state while dashed levels denote ‘vertical’ energy of the absorbing/fluorescing state computed at the optimized geometry of the respective doorway state. Numbers denote energy(eV)/dipole moment(Debye) of a given state. Dotted lines denote a diabatic correlation between states and solid/dashed arrows denote radiative/radiationless decay pathways, respectively.

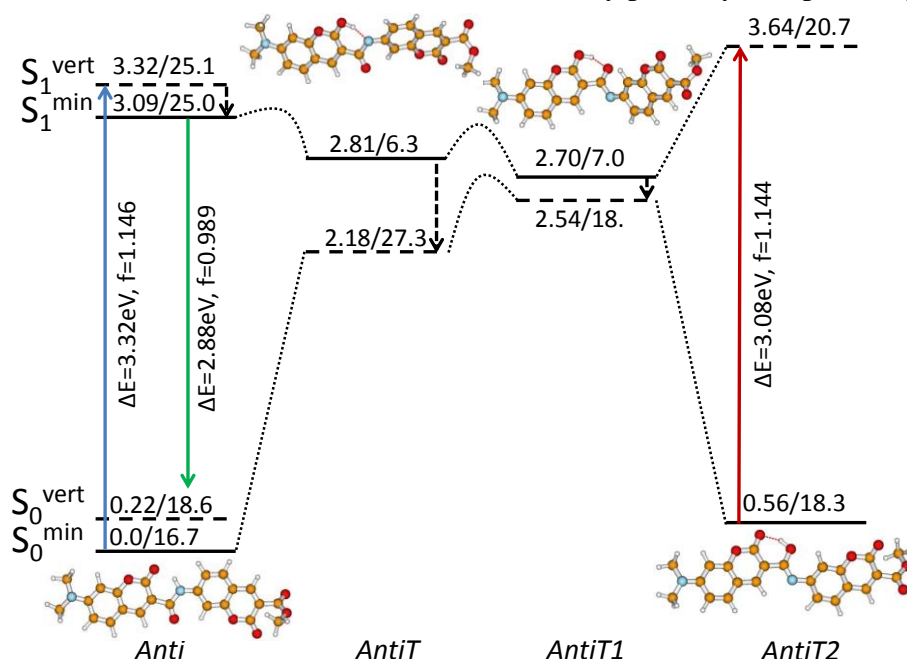


**Figure SF4.** Photophysical scheme of **Amide-7** related to the ESIPT process computed at the MP2/ADC(2) level of theory. Solid levels denote adiabatic (optimized) energy of a given state while dashed levels denote ‘vertical’ energy of the absorbing/fluorescing state computed at the optimized geometry of the respective doorway state. Numbers denote energy(eV)/dipole moment(Debye) of a given state. Dotted lines denote a diabatic correlation between states and solid/dashed arrows denote radiative/radiationless decay pathways, respectively.

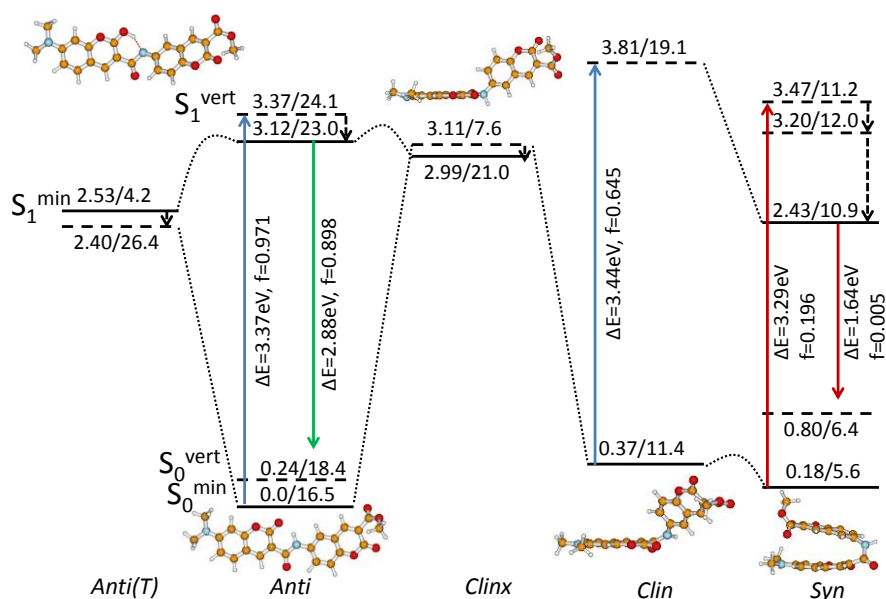


**Figure SF5.** Photophysical scheme of **Amide-6(A)** computed at the MP2/ADC(2) level of theory. Solid levels denote adiabatic (optimized) energy of a given state while dashed levels denote ‘vertical’ energy of the absorbing/fluorescing state computed at the optimized geometry of the respective doorway state. Numbers denote energy(eV)/dipole moment(Debye) of a given state. Dotted lines denote a diabatic correlation between states and solid/dashed arrows denote radiative/radiationless decay pathways, respectively.

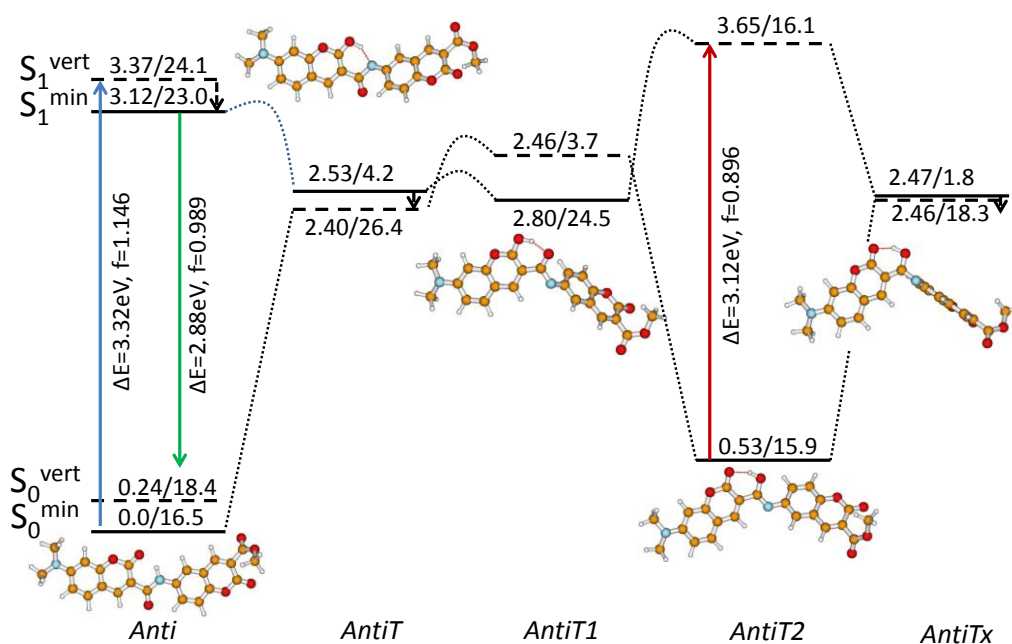


**Figure SF6.** Photophysical scheme of **Amide-6** related to the ESIPT process computed at the MP2/ADC(2) level of theory. Solid levels denote adiabatic (optimized) energy of a given state while dashed levels denote ‘vertical’ energy of the absorbing/fluorescing state computed at the optimized geometry of the respective doorway state. Numbers denote energy(eV)/dipole moment(Debye) of a given state. Dotted lines denote a diabatic correlation between states and solid/dashed arrows denote radiative/radiationless decay pathways, respectively.



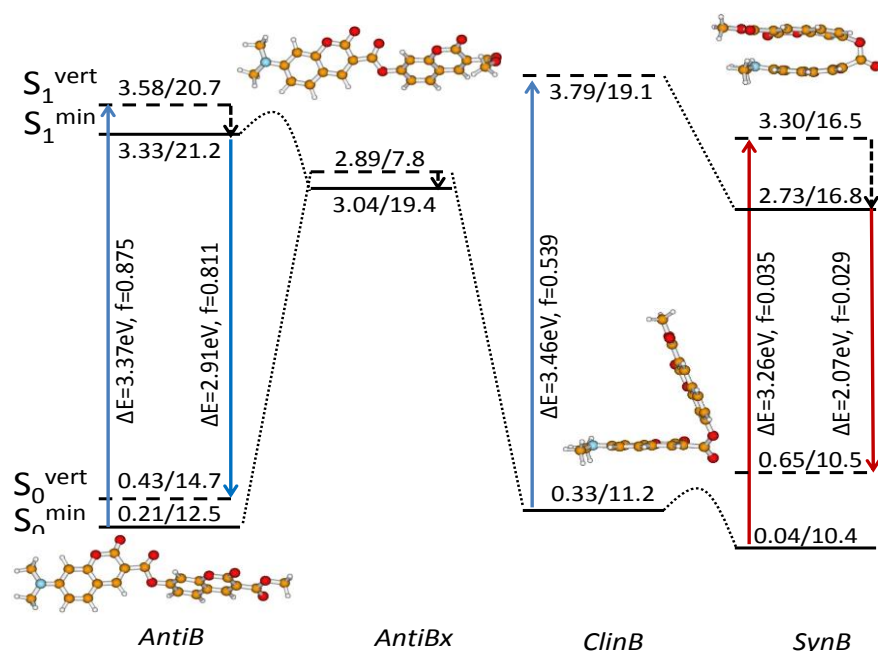


**Figure SF7.** Photophysical scheme of **Ester-7(B)** computed at the MP2/ADC(2) level of theory. Solid levels denote adiabatic (optimized) energy of a given state while dashed levels denote 'vertical' energy of the absorbing/fluorescing state computed at the optimized geometry of the respective doorway state. Numbers denote energy (eV)/dipole moment (Debye) of a given state. Dotted lines denote a diabatic correlation between states and solid/dashed arrows denote radiative/radiationless decay pathways, respectively.

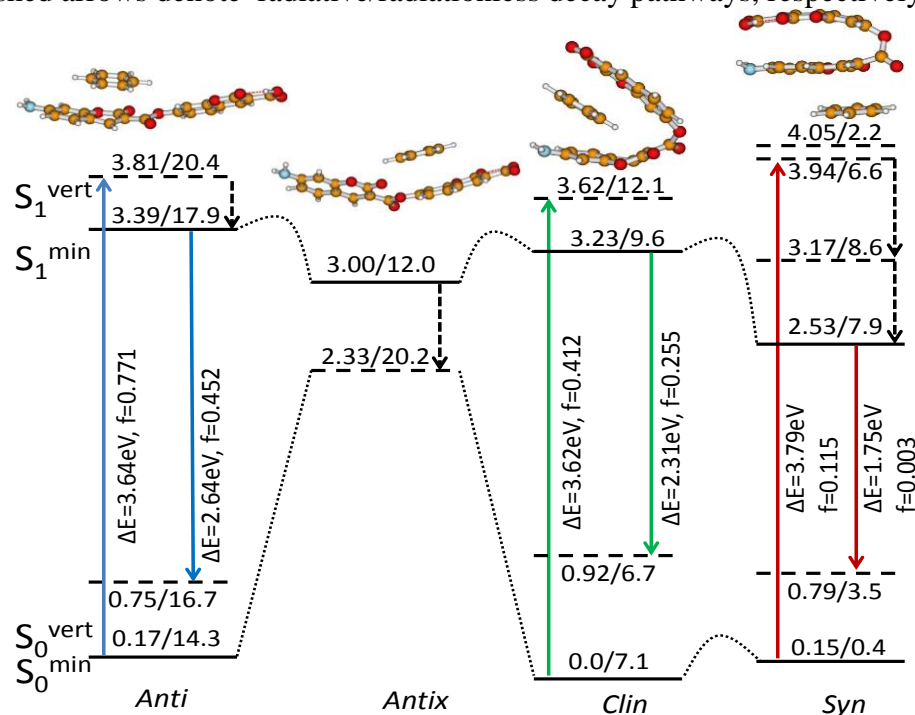


**Figure SF8.** Photophysical scheme of the **Ester-7 (trunk)** complexed with a single benzene molecule computed at the MP2/ADC(2)/def-SV(P) level of theory. Solid levels denote adiabatic (optimized) energy of a given state while dashed levels denote 'vertical' energy of the absorbing/fluorescing state computed at the optimized geometry of the respective doorway state. Numbers denote energy(eV)/dipole moment(Debye) of a given state. Dotted lines denote a diabatic correlation between states and solid/dashed arrows denote radiative/radiationless decay pathways, respectively.

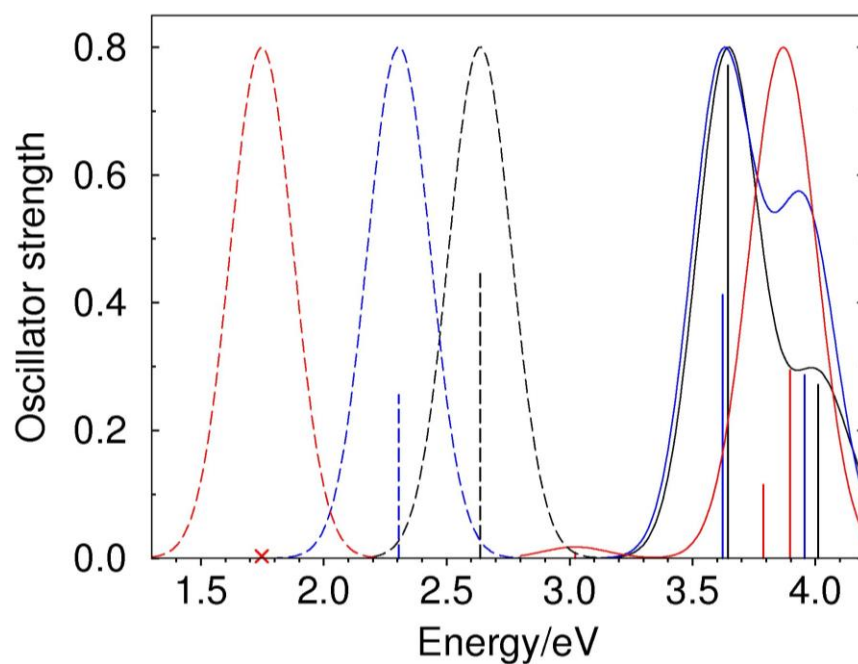


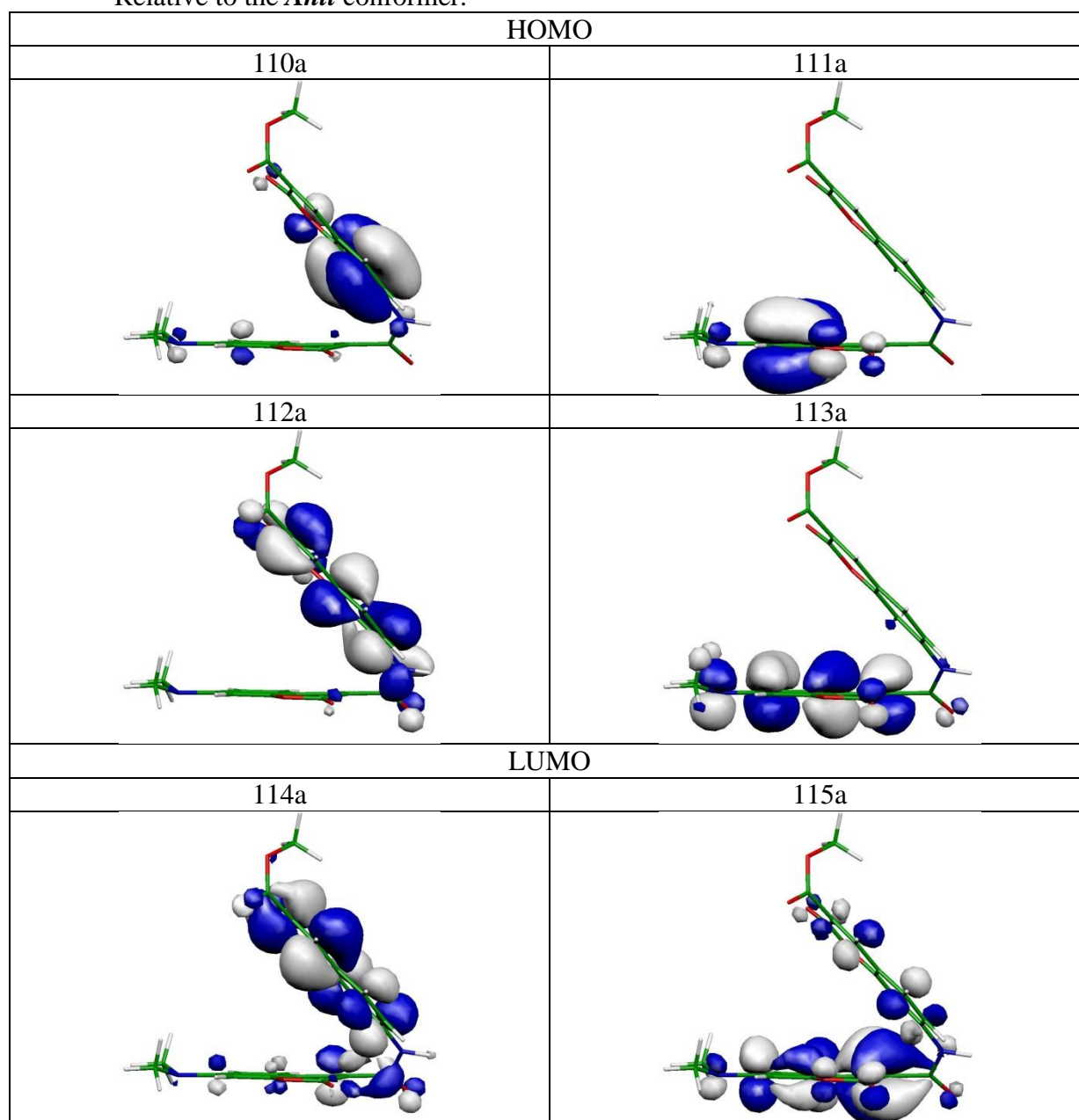
**Figure SF9.** Absorption (solid) and fluorescence (dashed) spectra computed at the MP2/ADC(2)/def-SV(P) level of theory for: *Anti* - black, *Clin* - blue, and *Syn* - red conformers of the **Ester-7(trunk)** complexed with a single benzene molecule. The computed “stick” spectra were convoluted with Gaussian function of 0.3eV FWHM and with the maximum normalized to 0.8.

**Table ST1.** Transition energy ( $\Delta E$ ), oscillator strength ( $f$ ), dipole moment ( $\mu$ ), leading electronic configurations, and relevant molecular orbitals of **Amide-7** computed with ADC(2)/cc-pVDZ method at the ground-state MP2/cc-pVDZ equilibrium.

(a) *Clin*

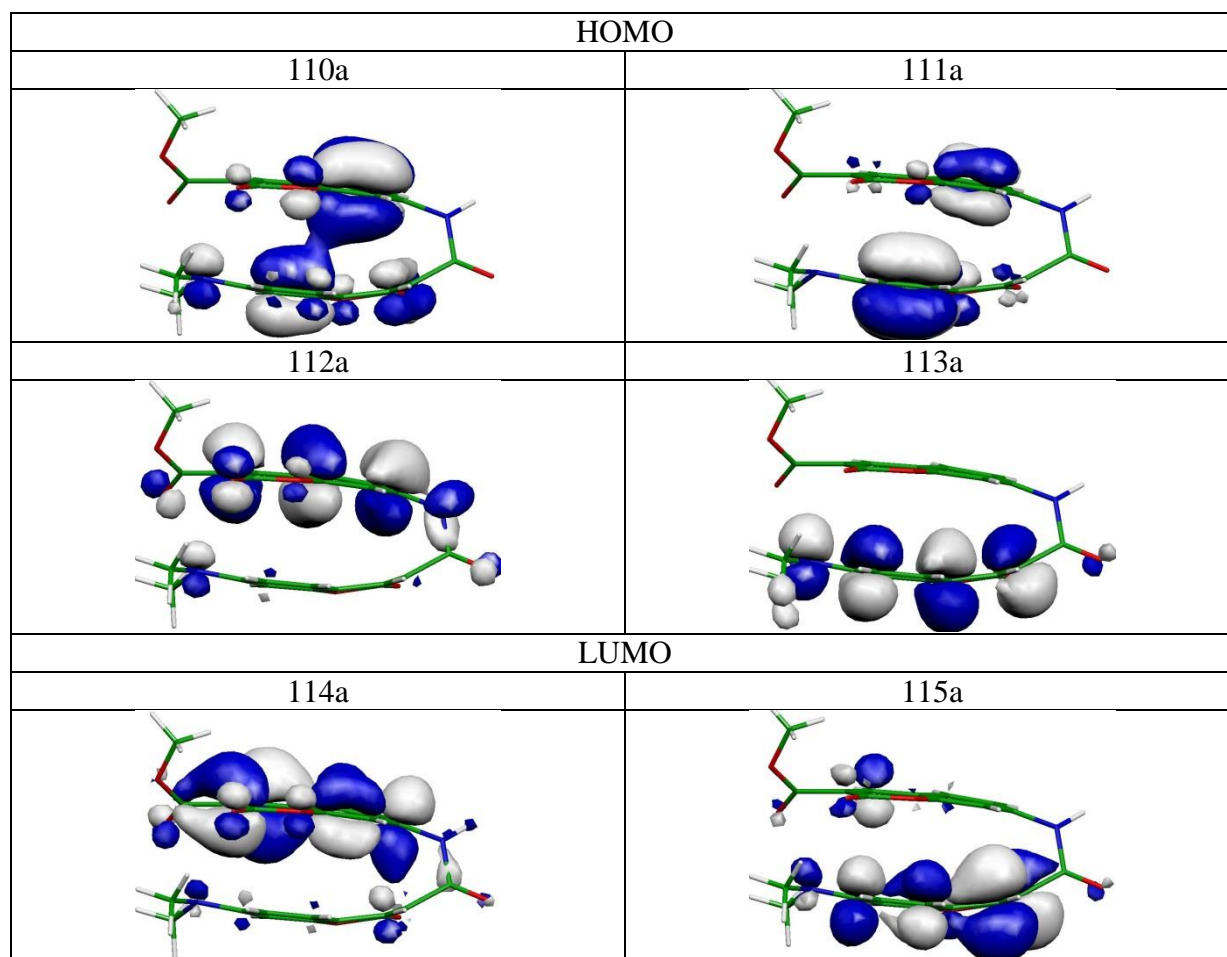
State	$\Delta E$ /eV	$f$	$\mu$ /Debye	el. config.
$S_0$	(0.39) <sup>1</sup>	-	4.20	(113a) <sup>2</sup>
$^1\pi\pi^*$	3.42	0.491	10.30	0.82(113a-115a)-0.45(113a-114a)
$^1\pi\pi^*$	3.84	0.455	6.07	0.83(112a-114a)
$^1n\pi^*$	4.16	0.021	8.83	0.47(111a-115a)-0.42(113a-114a)+0.41(110a-114a)
$^1\pi\pi^*$	4.21	0.038	7.69	0.55(111a-115a)-0.36(110a-114a)-0.36(113a-117a)-0.32(111a-114a)

<sup>1)</sup> Relative to the *Anti* conformer.



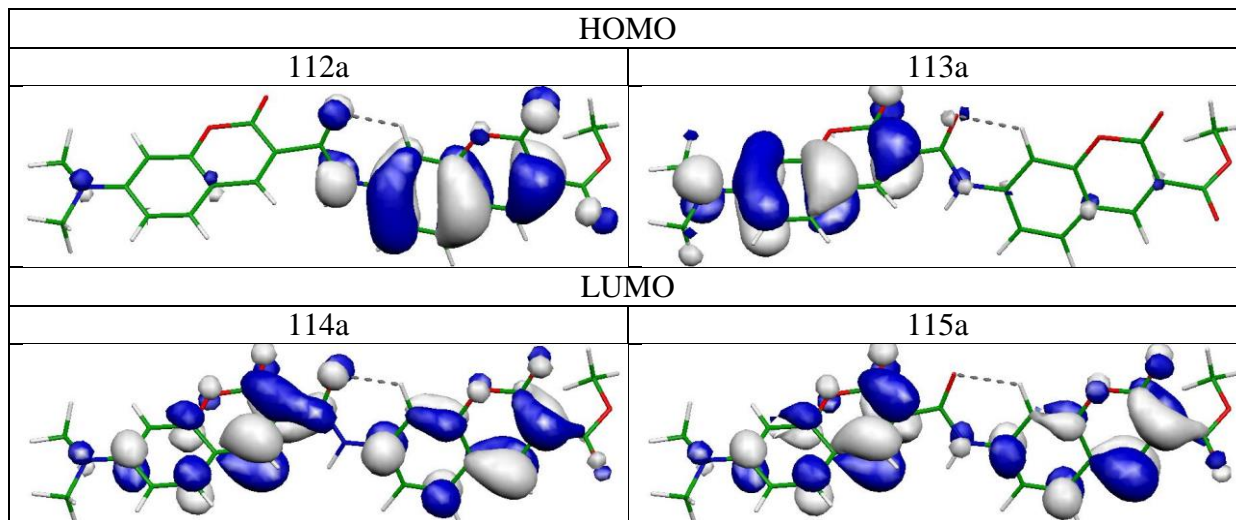
(b) *Syn*

State	$\Delta E/\text{eV}$	f	$\mu/\text{Debye}$	el. config.
$S_0$	$(0.20)^1$	-	5.21	$(113a)^2$
$^1\pi\pi^*$	3.02	0.062	10.83	0.95(113a-114a)
$^1\pi\pi^*$	3.37	0.097	10.37	0.87(113a-115a)
$^1n\pi^*$	3.74	0.404	4.65	0.78(112a-114a)
$^1\pi\pi^*$	4.03	0.065	3.69	0.65(110a-114a)-0.45(111a-114a)



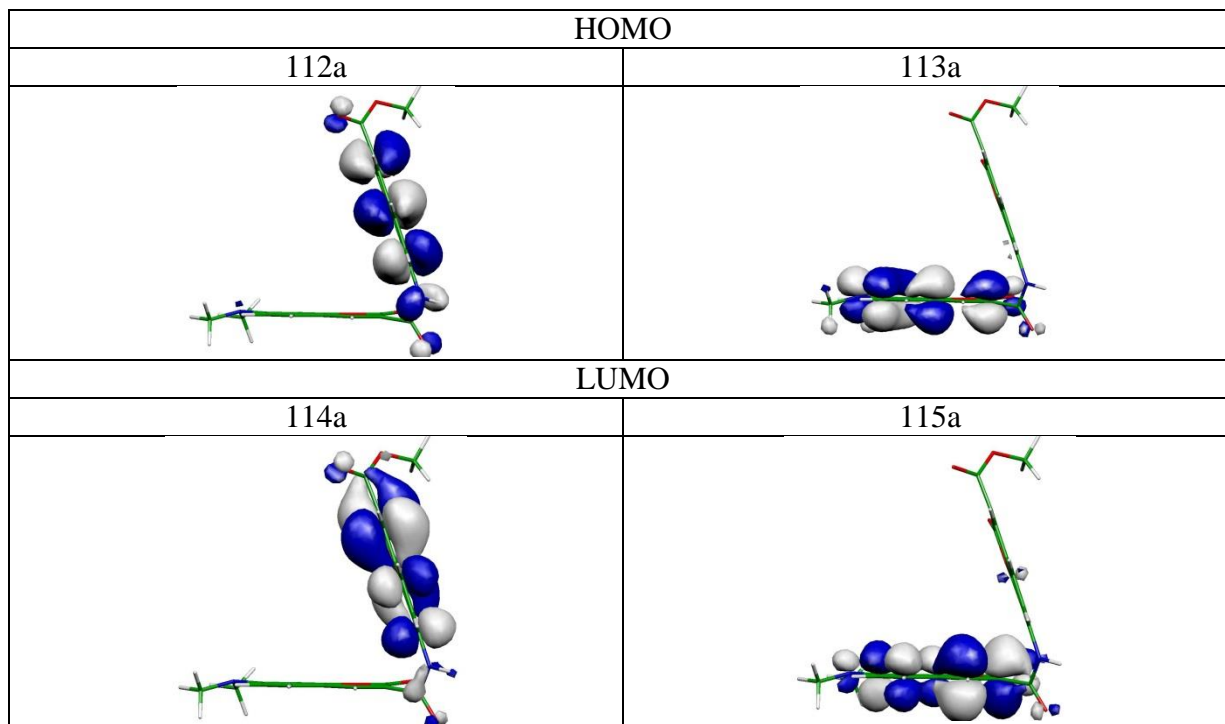
(c) *AntiB*

State	$\Delta E/eV$	f	$\mu/Debye$	el. config.
$S_0$	$(0.45)^1$	-	15.88	$(113a)^2$
$^1\pi\pi^*$	3.52	0.970	24.72	$0.77(113a-114a)+0.52(113a-115a)$
$^1\pi\pi^*$	3.86	0.274	17.06	$0.69(112a-114a)-0.48(112a-115a)$



(d) *ClinB*

State	$\Delta E/eV$	f	$\mu/Debye$	el. config.
$S_0$	$(0.50)^1$	-	7.09	$(113a)^2$
$^1\pi\pi^*$	3.56	0.521	12.47	$0.94(113a-115a)$
$^1\pi\pi^*$	3.89	0.399	7.25	$0.84(112a-114a)$



(e) *SynB*

State	$\Delta E$ /eV	f	$\mu$ /Debye	el. config.
$S_0$	(0.25) <sup>1</sup>	-	8.18	(113a) <sup>2</sup>
$^1\pi\pi^*$	2.91	0.007	11.06	0.96(113a-114a)
$^1\pi\pi^*$	3.28	0.203	14.06	0.92(113a-115a)
$^1\pi\pi^*$	3.71	0.322	6.32	0.81(112a-114a)

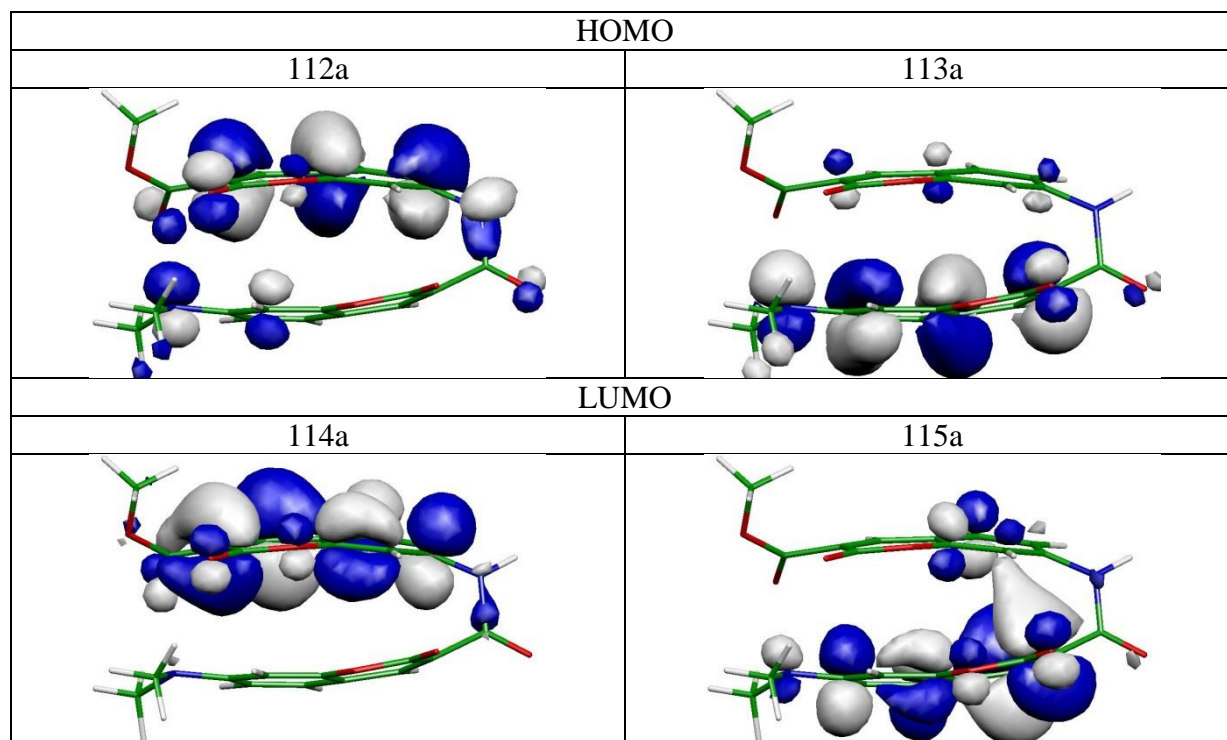


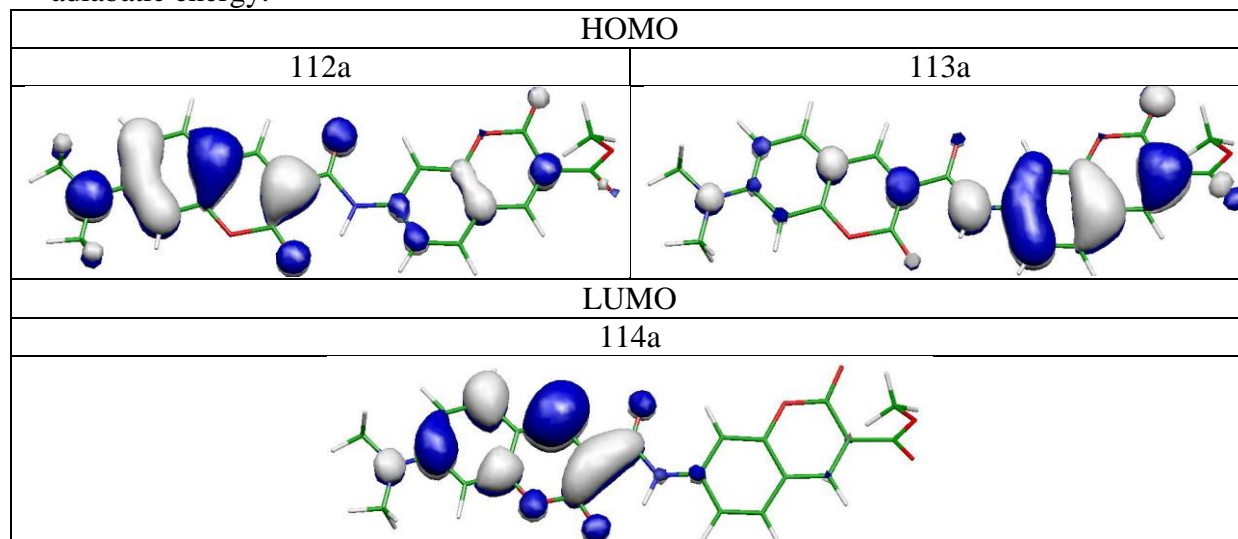


**Table ST2.** Vertical fluorescence energy ( $\Delta E$ ), oscillator strength ( $f$ ), dipole moment ( $\mu$ ), leading electronic configurations, and relevant molecular orbitals computed at the equilibrium of the  $S_1$  state of **Amide-7**.

(a) *Anti*

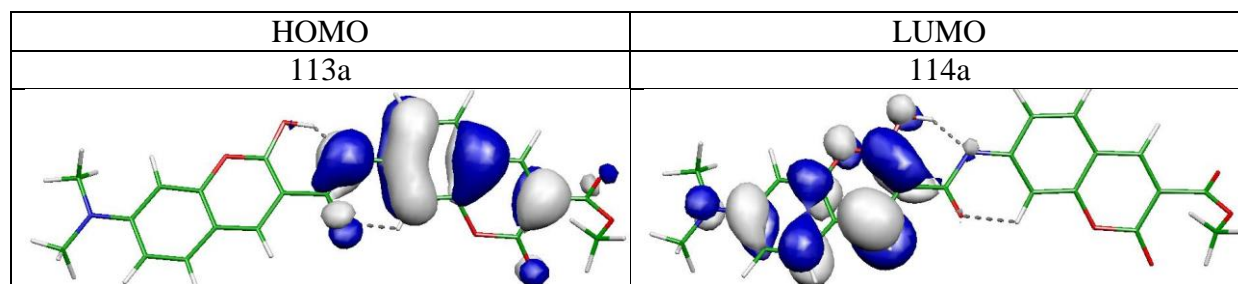
State	$\Delta E/\text{eV}$	$f$	$\mu/\text{Debye}$	Electronic Configuration
$S_0$	2.87	0.989	18.64	$(113a)^2$
$S_1$	$(3.09)^1$	-	25.03	$0.77(112a-114a)-0.56(113a-114a)$

<sup>1)</sup> adiabatic energy.



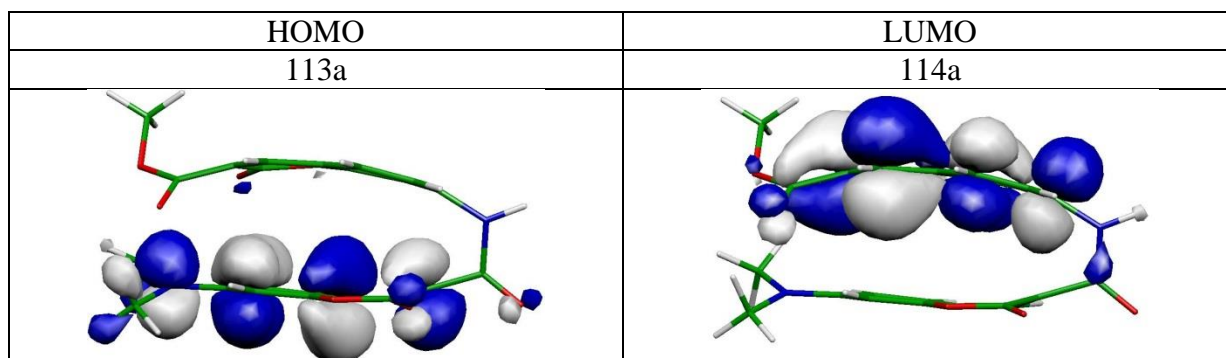
(b) *AntiT*

State	$\Delta E/\text{eV}$	$\mu/\text{Debye}$	Electronic Configuration
$S_0$	0.63	27.32	$(113a)^2$
$S_1$	$(2.81)^1$	6.26	$0.91(113a-114a)$



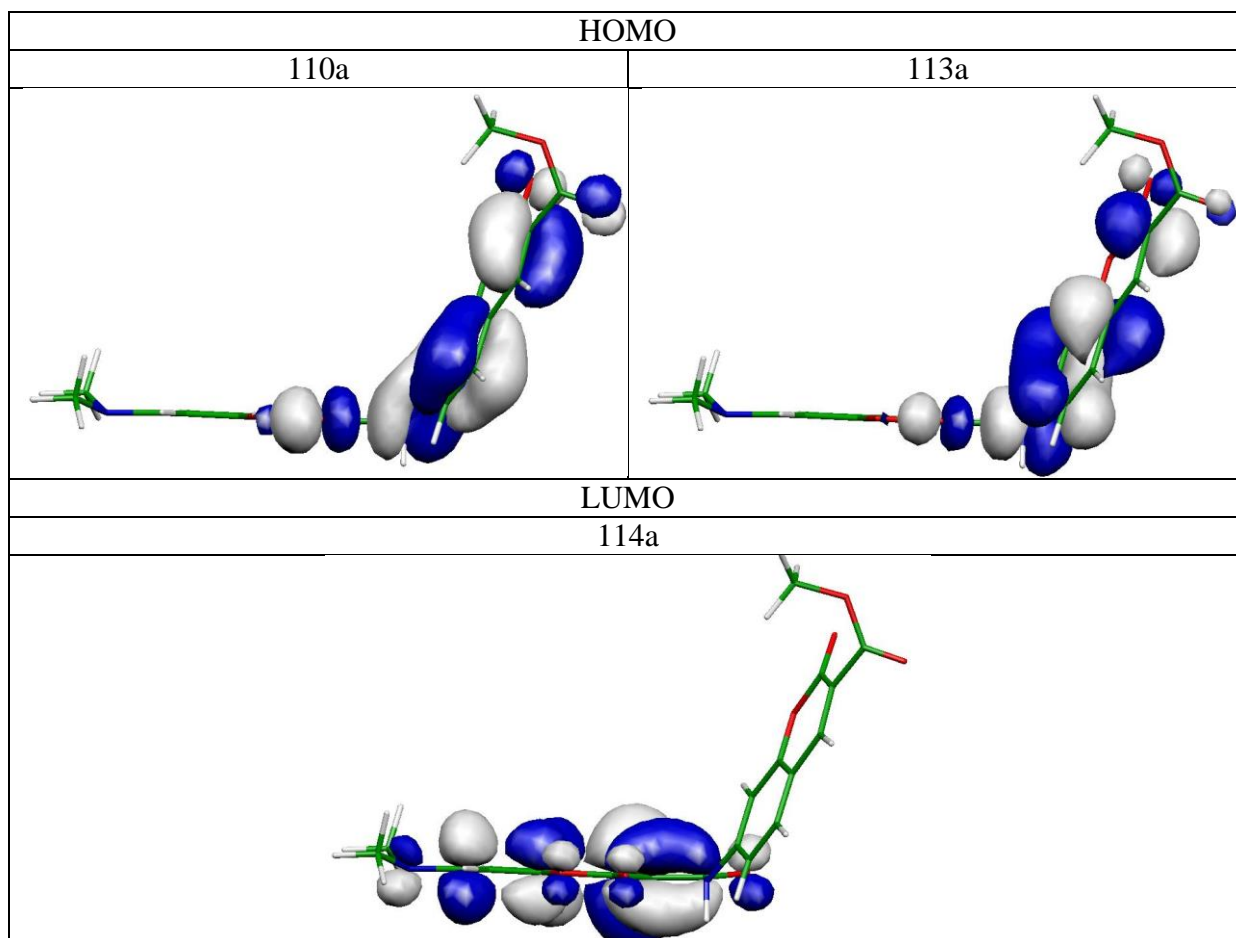
(c) *Syn*

State	$\Delta E/\text{eV}$	f	$\mu/\text{Debye}$	Electronic Configuration
$S_0$	1.53	0.005	6.96	$(113a)^2$
$S_1$	$(2.43)^1$	-	11.96	$0.97(113a-114a)$



(d) *Clinx*

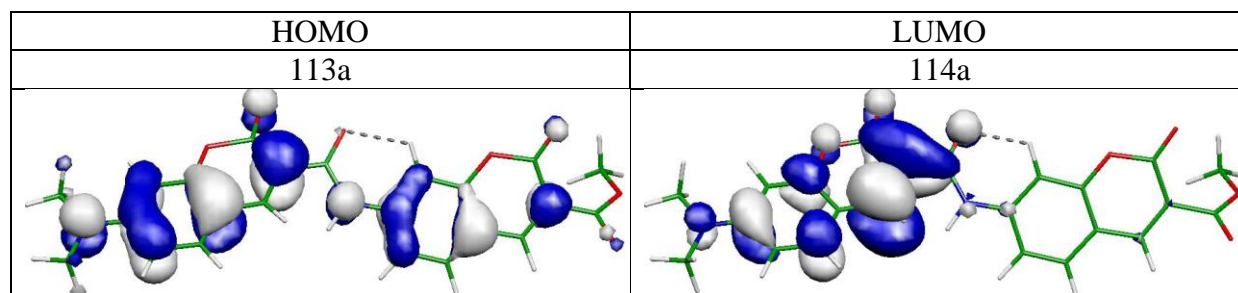
State	$\Delta E/\text{eV}$	$\mu/\text{Debye}$	Electronic Configuration
$S_0$	0.03	20.05	$(113a)^2$
$S_1$	$(3.12)^1$	10.77	$0.74(113a-114a)+0.53(110a-114a)$





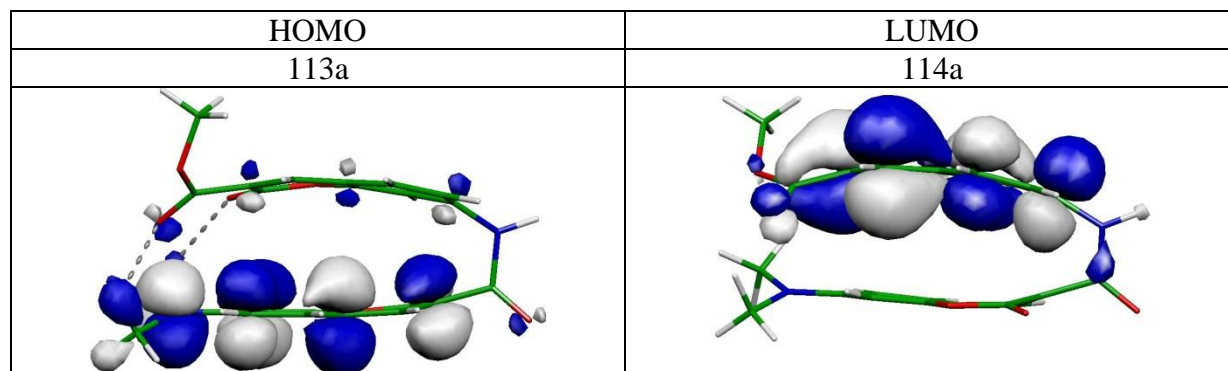
(e) *Anti*

State	$\Delta E/\text{eV}$	f	$\mu/\text{Debye}$	Electronic Configuration
$S_0$	2.84	0.786	18.24	$(113a)^2$
$S_1$	$(3.64)^1$	-	25.97	0.87(113a-114a)



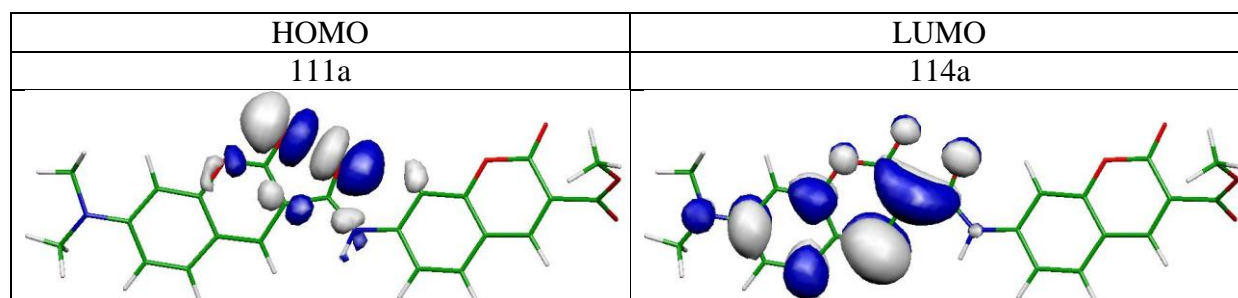
(f) *Syn*

State	$\Delta E/\text{eV}$	f	$\mu/\text{Debye}$	Electronic Configuration
$S_0$	0.96	0.001	11.56	$(113a)^2$
$S_1$	$(2.41)^1$	-	13.11	0.92(113a-114a)



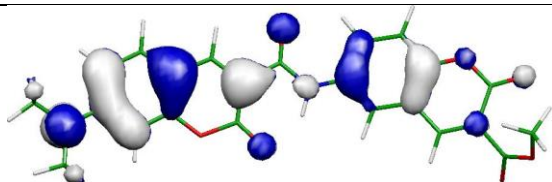
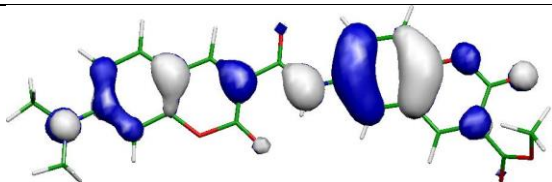
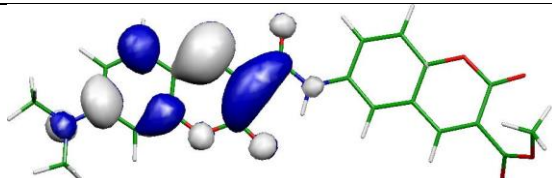
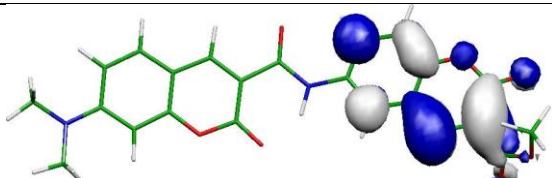
(g) *AntiBx*

State	$\Delta E/\text{eV}$	$\mu/\text{Debye}$	Electronic Configuration
$S_0$	-0.48	20.14	$(113a)^2$
$S_1$	$(2.61)^1$	8.89	0.97(111a-114a)



**Table ST3.** Transition energy ( $\Delta E$ ), oscillator strength ( $f$ ), dipole moment ( $\mu$ ), leading electronic configurations, and relevant molecular orbitals of **Amide-6** computed with ADC(2)/cc-pVDZ method at the ground-state MP2/cc-pVDZ equilibrium.

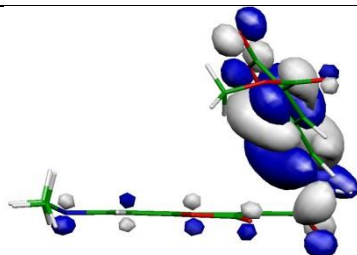
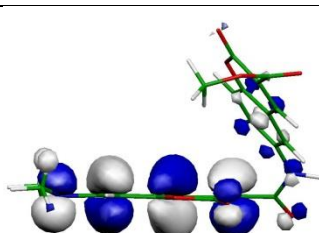
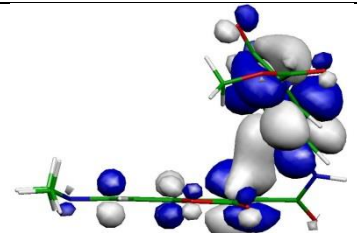
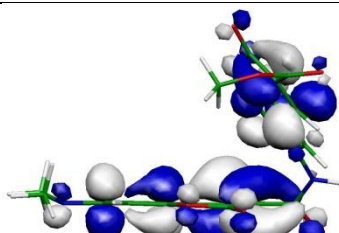
(a) *Anti*

State	$\Delta E$ /eV	f	$\mu$ /Debye	el. config.
$S_0$	-	-	16.49	$(113a)^2$
$^1\pi\pi^*$	3.37	0.971	24.14	$0.70(112a-114a)-0.65(113a-114a)$
$^1\pi\pi^*$	3.54	0.068	23.21	$0.83(113a-115a)+0.44(112a-115a)$
$^1\pi\pi^*$	4.00	0.092	6.11	$0.63(113a-114a)+0.60(112a-114a)$
HOMO				
112a			113a	
				
LUMO				
114a			115a	
				

(b) *Clin*

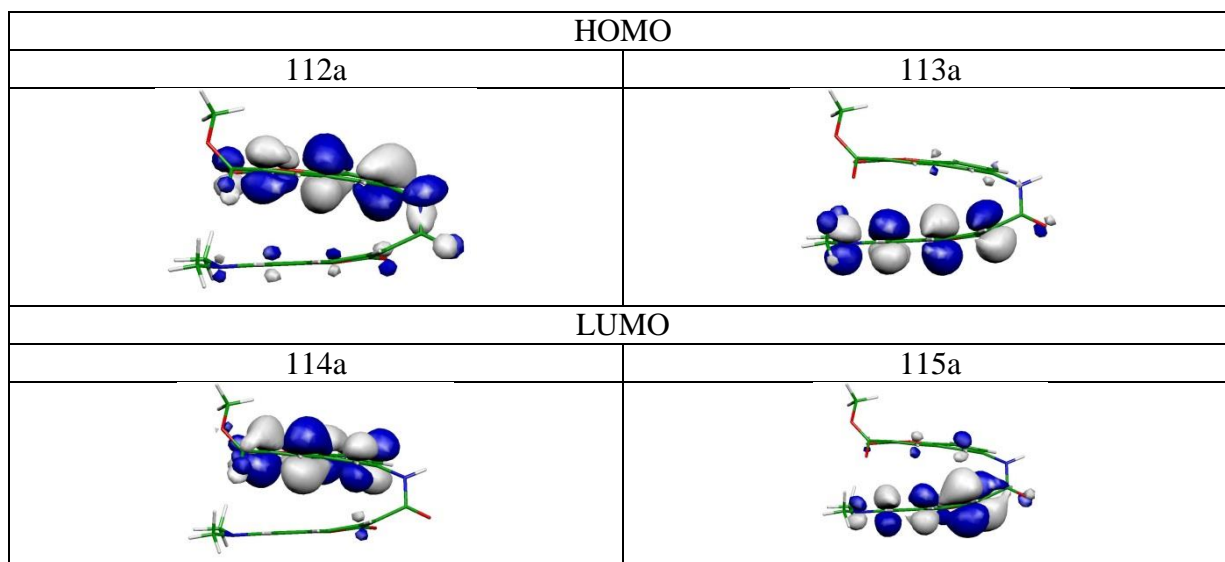
State	$\Delta E$ /eV	$f$	$\mu$ /Debye	el. config.
$S_0$	$(0.37)^1$	-	11.48	$(113a)^2$
$^1\pi\pi^*$	3.44	0.645	19.11	$0.71(113a-114a)-0.81(113a-115a)$
$1\pi\pi^*$	3.67	0.089	15.42	$0.85(112a-114a)$

<sup>1)</sup> Relative to *Anti* conformer.

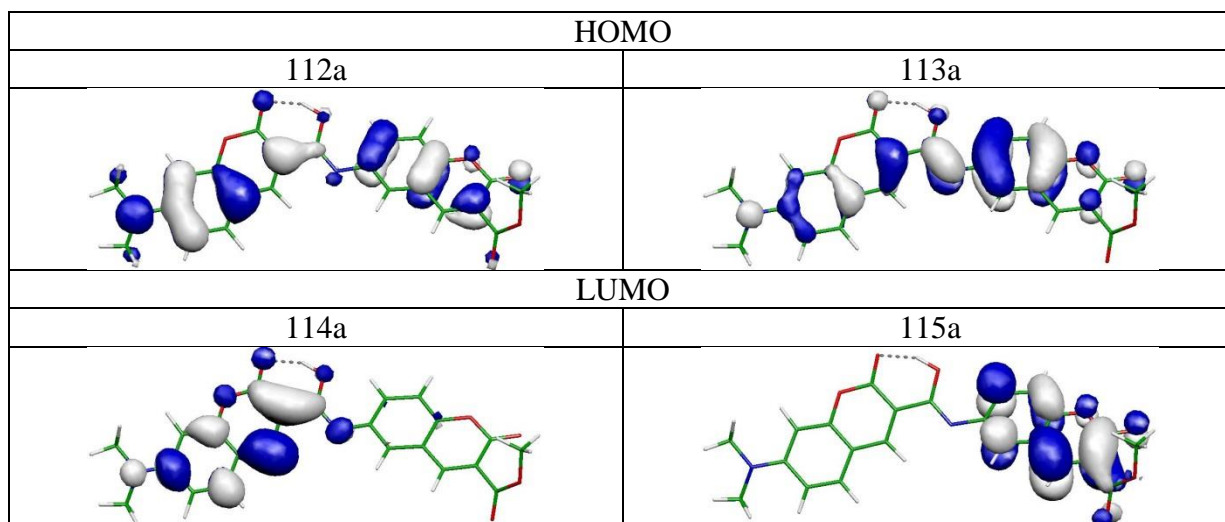
Relative to 111a conformer.	
HOMO	
112a	113a
	
LUMO	
114a	115a
	

(c) *Syn*

State	$\Delta E$ /eV	f	$\mu$ /Debye	el. config.
$S_0$	(0.18) <sup>1</sup>	-	5.58	(113a) <sup>2</sup>
$^1\pi\pi^*(CT)$	3.02	0.087	11.96	0.93(113a-114a)
$^1\pi\pi^*(LE)$	3.29	0.197	11.17	0.90(113a-115a)
$^1\pi\pi^*(LE)$	3.65	0.130	3.12	0.89(112a-114a)

*AntiT2*

State	$\Delta E$ /eV	f	$\mu$ /Debye	el. config.
$S_0$	(0.53) <sup>1</sup>	-	15.93	(113a) <sup>2</sup>
$^1\pi\pi^*$	3.12	0.896	16.13	0.85(113a-114a)-0.46(112a-114a)
$^1\pi\pi^*$	3.56	0.084	22.65	0.87(113a-115a)+0.35(112a-115a)
$^1\pi\pi^*$	3.79	0.035	5.96	0.74(112a-114a)+0.39(113a-114a)

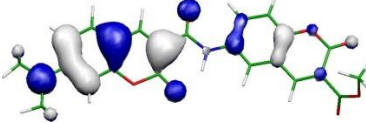
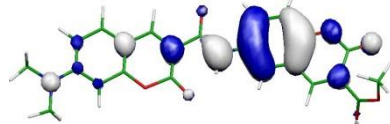
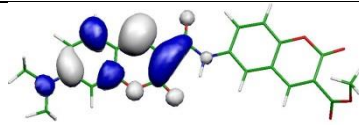


**Table ST4.** Vertical fluorescence energy ( $\Delta E$ ), oscillator strength ( $f$ ), dipole moment ( $\mu$ ), leading electronic configurations, and relevant molecular orbitals computed at the equilibrium of the S1 state of **Amide-6**.

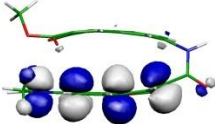
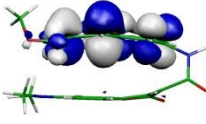
(a) *Anti*

State	$\Delta E/\text{eV}$	$f$	$\mu/\text{Debye}$	Electronic Configuration
$S_0$	2.89	0.989	18.36	$(113a)^2$
$S_1$	$(3.12)^1$	-	22.98	$0.75(112a-114a)-0.61(113a-114a)$

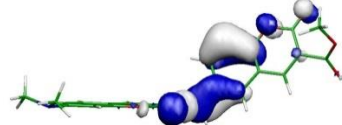
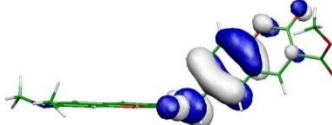
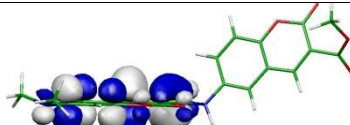
<sup>1)</sup> adiabatic energy.

HOMO	
112a	113a
	
LUMO	
114a	
	

(b) *Syn*

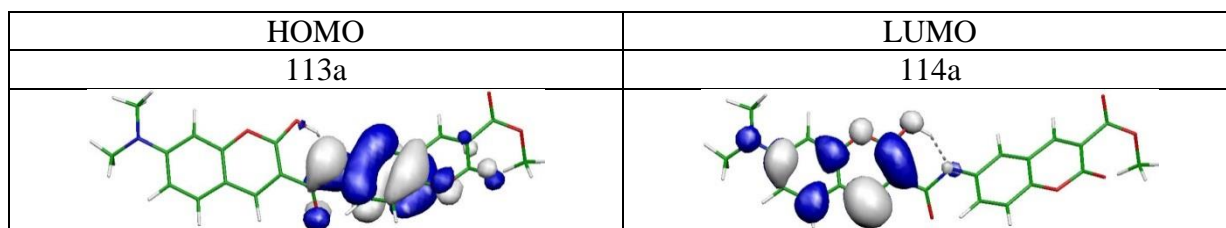
State	$\Delta E/\text{eV}$	$f$	$\mu/\text{Debye}$	Electronic Configuration
$S_0$	1.64	0.005	6.38	$(113a)^2$
$S_1$	$(2.43)^1$	-	10.85	$0.96(113a-114a)$
HOMO		LUMO		
113a		114a		
				

(c) *Clinx*

State	$\Delta E/\text{eV}$	$\mu/\text{Debye}$	Electronic Configuration
$S_0$	-0.12	21.00	$(113a)^2$
$S_1$	$(2.98)^1$	7.55	$0.78(113a-114a)+0.51(110a-114a)$
HOMO			
110a		113a	
			
LUMO			
114a			
			

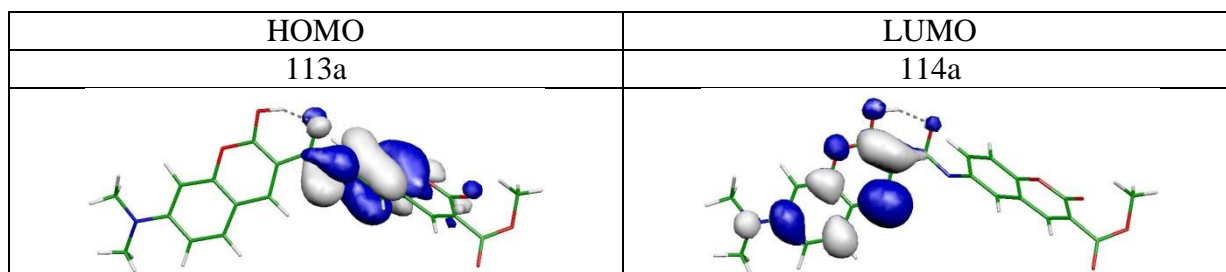
(d) *AntiT*

State	$\Delta E/\text{eV}$	$\mu/\text{Debye}$	Electronic Configuration
$S_0$	0.13	26.35	$(113a)^2$
$S_1$	$(2.53)^1$	4.21	$0.92(113a-114a)$



(e) *AntiT1*

State	$\Delta E/\text{eV}$	$\mu/\text{Debye}$	Electronic Configuration
$S_0$	-0.34	24.53	$(113a)^2$
$S_1$	$(2.46)^1$	3.72	$0.92(113a-114a)$



(f) *AntiTx*

State	$\Delta E/\text{eV}$	$\mu/\text{Debye}$	Electronic Configuration
$S_0$	0.01	18.30	$(113a)^2$
$S_1$	$(2.47)^1$	1.75	$0.91(113a-114a)$

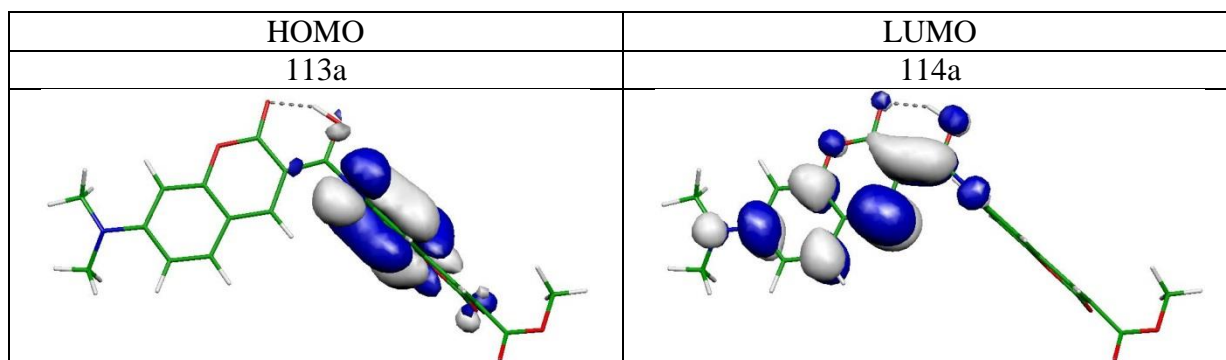
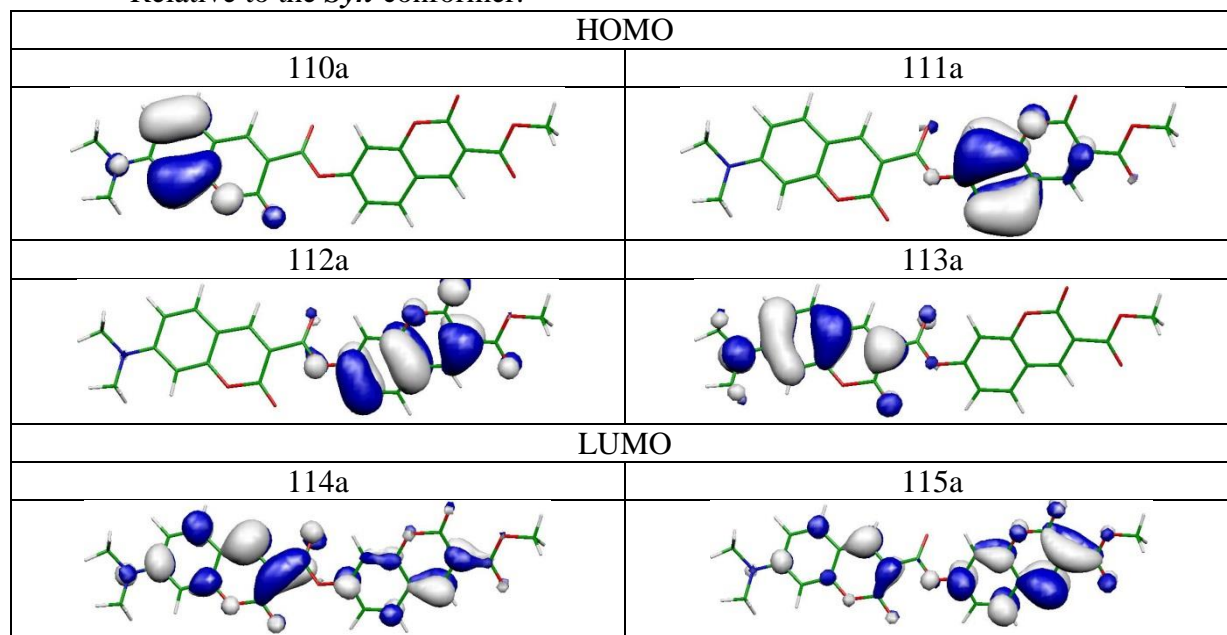


**Table ST5.** Transition energy ( $\Delta E$ ), oscillator strength ( $f$ ), dipole moment ( $\mu$ ), leading electronic configurations, and relevant molecular orbitals of **Ester-7** computed with ADC(2)/cc-pVDZ method at the ground-state MP2/cc-pVDZ equilibrium.

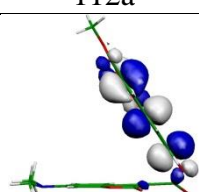
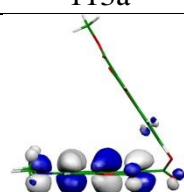
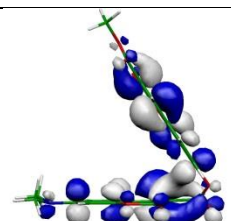
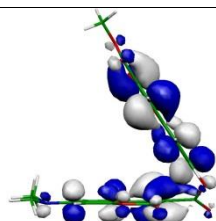
(a) *Anti*

State	$\Delta E$ /eV	$f$	$\mu$ /Debye	el. config.
$S_0$	(0.16) <sup>1</sup>	-	10.70	(113a) <sup>2</sup>
$^1\pi\pi^*$	3.36	0.934	19.78	0.87(113a-114a)+0.40(113a-115a)
$^1\pi\pi^*$	3.84	0.206	13.77	0.67(112a-115a)-0.55(112a-114a)
$^1\pi\pi^*$	4.11	0.004	16.45	0.76(110a-114a)+0.41(110a-115a)-0.41(113a-116a)

<sup>1)</sup> Relative to the *Syn* conformer.

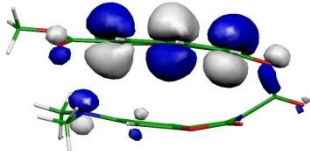
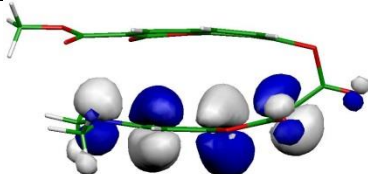
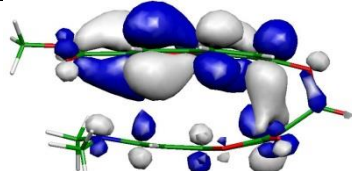
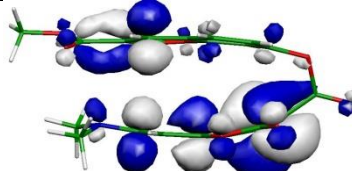


(b) *Clin*

State	$\Delta E$ \eV	f	$\mu$ /Debye	el. config.
$S_0$	(0.22) <sup>1</sup>	-	7.24	(113a) <sup>2</sup>
<sup>1</sup> $\pi\pi^*$	3.34	0.526	16.11	0.77(113a-114a)-0.56(113a-115a)
<sup>1</sup> $\pi\pi^*$	3.81	0.324	8.36	0.63(112a-115a)+0.63(112a-114a)
HOMO				
112a			113a	
				
LUMO				
114a			115a	
				

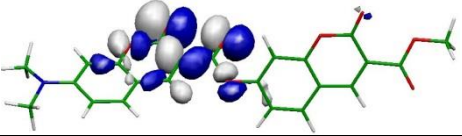
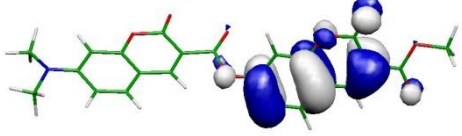
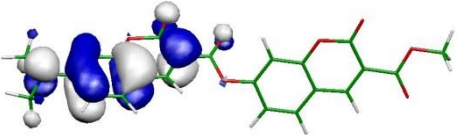
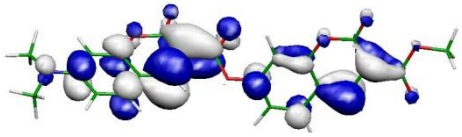
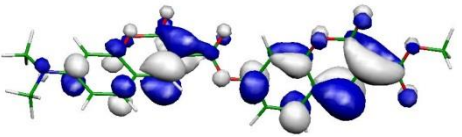


(c) *Syn*

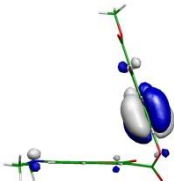
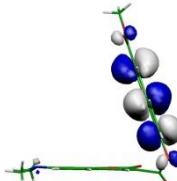
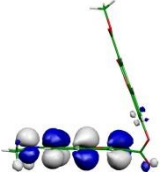
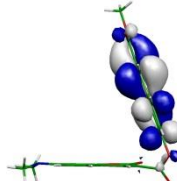
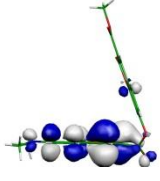
State	$\Delta E$ /eV	f	$\mu$ /Debye	el. config.
$S_0$	-	-	7.43	(113a) <sup>2</sup>
$^1\pi\pi^*$	3.19	0.165	14.78	0.85(113a-114a)-0.44(113a-115a)
$^1\pi\pi^*$	3.45	0.022	13.90	0.75(113a-115a)+0.42(113a-114a)- 0.40(112a-114a)
$^1\pi\pi^*$	3.79	0.317	6.48	0.74(112a-114a)
HOMO				
112a			113a	
				
LUMO				
114a			115a	
				

(d) *AntiB*

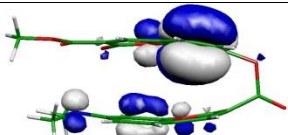
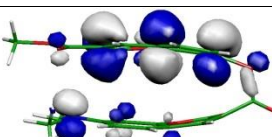
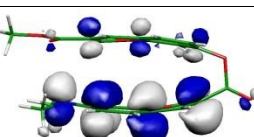
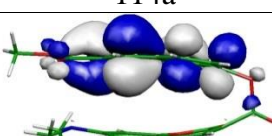
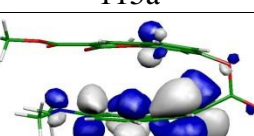
State	$\Delta E$ /eV	f	$\mu$ /Debye	el. config.
$S_0$	(0.21) <sup>1</sup>	-	12.47	(113a) <sup>2</sup>
$^1\pi\pi^*$	3.37	0.875	20.72	0.82(113a-114a)-0.50(113a-115a)
$^1\pi\pi^*$	3.87	0.209	13.70	0.62(112a-115a)+0.56(112a-114a)
$^1n\pi^*$	3.97	0.012	6.07	0.74(107a-114a)-0.47(107a-115a)

HOMO	
107a	
	
112a	113a
	
LUMO	
114a	115a
	

(e) *ClinB*

(c) ClinB				
State	$\Delta E$ /eV	f	$\mu$ /Debye	el. config.
$S_0$	(0.33) <sup>1</sup>	-	11.21	(113a) <sup>2</sup>
<sup>1</sup> $\pi\pi^*$	3.46	0.539	19.07	0.94(113a-115a)
<sup>1</sup> $\pi\pi^*$	3.87	0.326	10.21	0.86(112a-114a)-0.36(110a-114a)
HOMO				
110a				
				
112a			113a	
				
LUMO				
114a			115a	
				

(f) *SynB*

State	$\Delta E$ /eV	f	$\mu$ /Debye	el. config.
$S_0$	(0.04) <sup>1</sup>	-	10.38	(113a) <sup>2</sup>
<sup>1</sup> $\pi\pi^*$	3.26	0.035	16.52	0.95(113a-114a)
<sup>1</sup> $\pi\pi^*$	3.30	0.191	17.48	0.91(113a-115a)
<sup>1</sup> $\pi\pi^*$	3.77	0.290	8.40	0.83(112a-114a)-0.33(110a-114a)
HOMO				
110a				
				
112a			113a	
				
LUMO				
114a			115a	
				

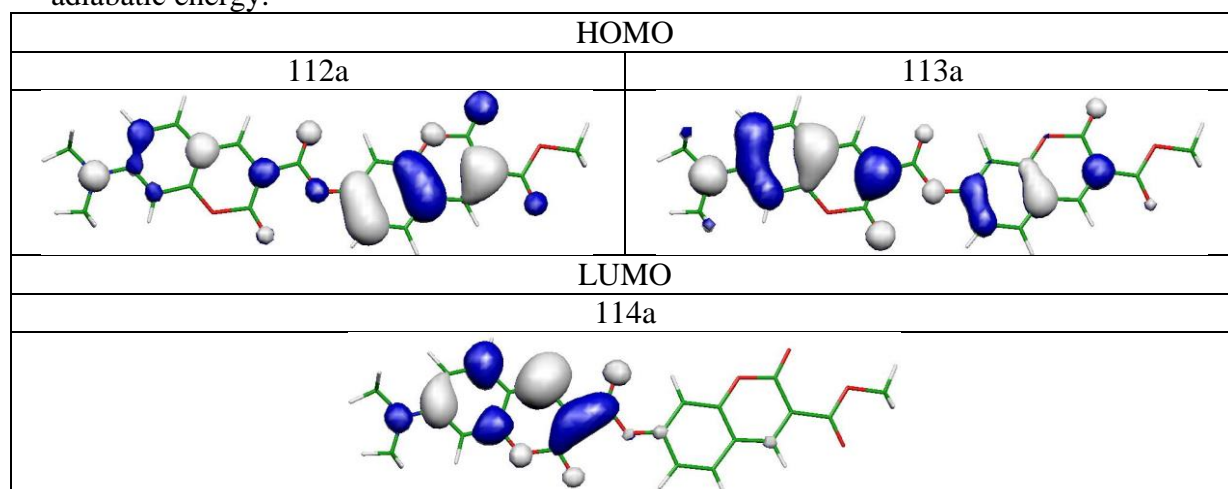


**Table ST6.** Vertical fluorescence energy ( $\Delta E$ ), oscillator strength ( $f$ ), dipole moment ( $\mu$ ), leading electronic configurations, and relevant molecular orbitals computed at the equilibrium of the  $S_1$  state of **Ester-7**.

(a) *Anti*

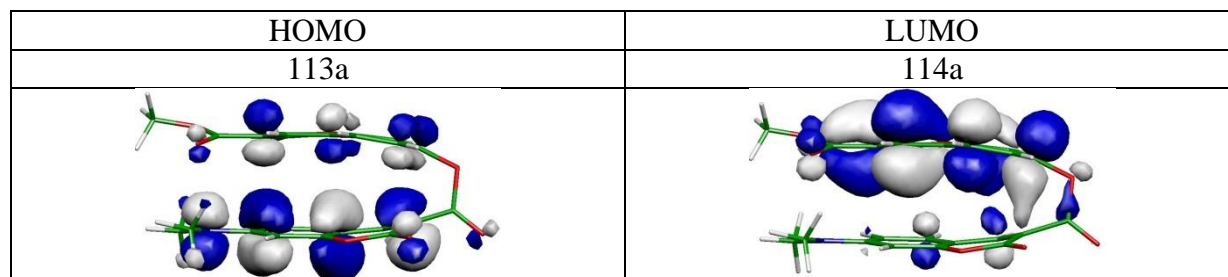
State	$\Delta E/\text{eV}$	$f$	$\mu/\text{Debye}$	Electronic Configuration
$S_0$	2.87	0.888	13.16	$(113a)^2$
$S_1$	$(3.26)^1$	-	19.88	$0.88(113a-114a)+0.38(112a-114a)$

<sup>1)</sup> adiabatic energy.



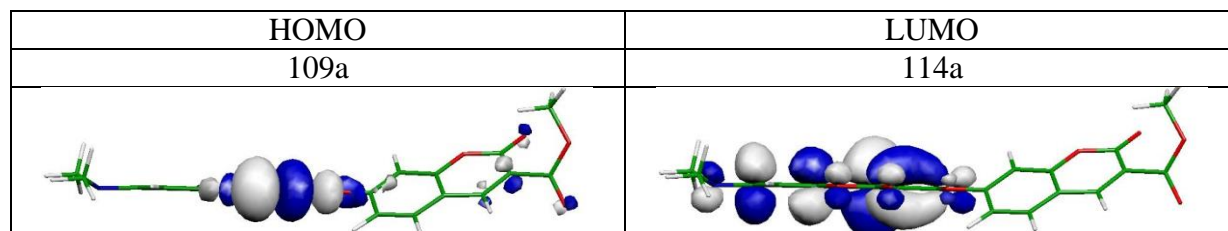
(b) *Syn*

State	$\Delta E/\text{eV}$	$f$	$\mu/\text{Debye}$	Electronic Configuration
$S_0$	1.83	0.003	7.94	$(113a)^2$
$S_1$	$(2.58)^1$	-	13.29	$0.97(113a-114a)$



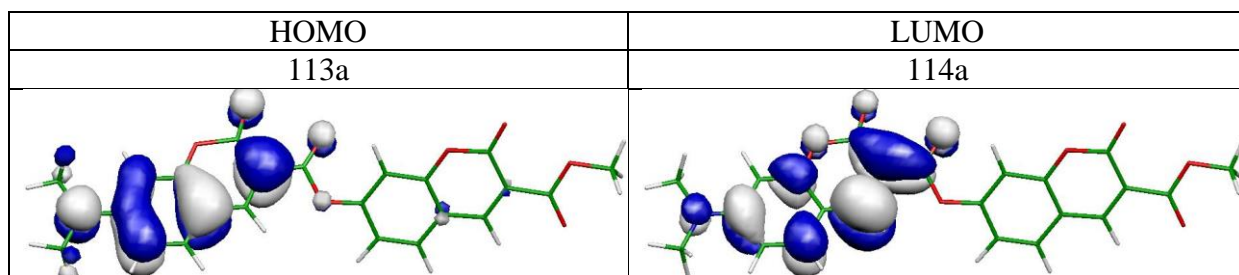
(c) *Antix*

State	$\Delta E/\text{eV}$	$\mu/\text{Debye}$	Electronic Configuration
$S_0$	0.72	18.63	$(113a)^2$
$S_1$	$(3.22)^1$	13.3	$0.94(109a-114a)$



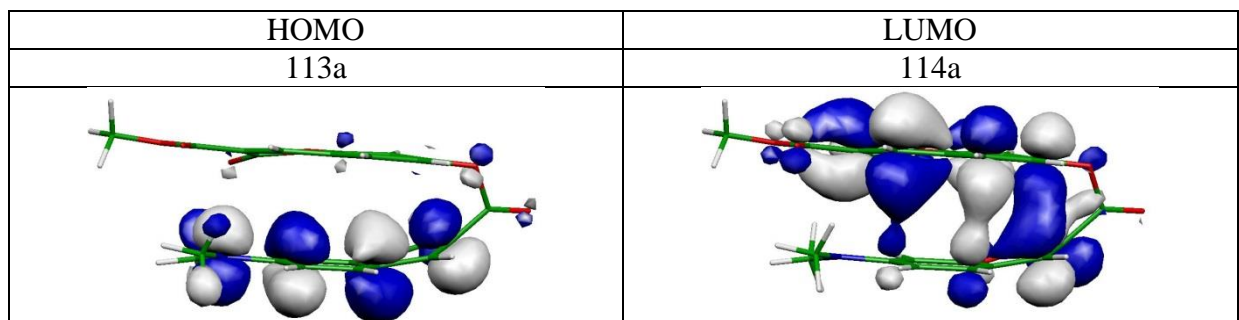
(d) *AntiB*

State	$\Delta E/\text{eV}$	f	$\mu/\text{Debye}$	Electronic Configuration
$S_0$	2.91	0.811	14.72	$(113a)^2$
$S_1$	$(3.33)^1$	-	21.19	$0.95(113a-114a)$



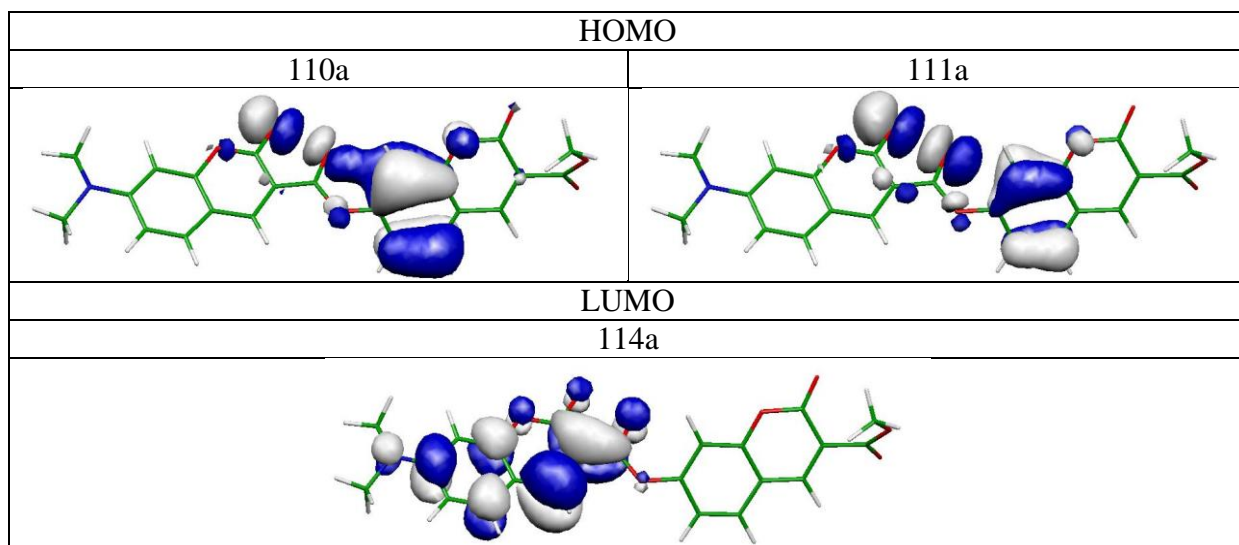
(e) *SynB*

State	$\Delta E/\text{eV}$	f	$\mu/\text{Debye}$	Electronic Configuration
$S_0$	2.07	0.029	10.53	$(113a)^2$
$S_1$	$(2.73)^1$	-	16.76	$0.93(113a-114a)$



(f) *AntiBx*

State	$\Delta E/\text{eV}$	$\mu/\text{Debye}$	Electronic Configuration
$S_0$	-0.15	19.38	$(113a)^2$
$S_1$	$(2.89)^1$	7.79	$0.83(111a-114a)+0.52(110a-114a)$



## 6. Experimental results

### 6.1 Photophysical Measurements of **Amide-7**

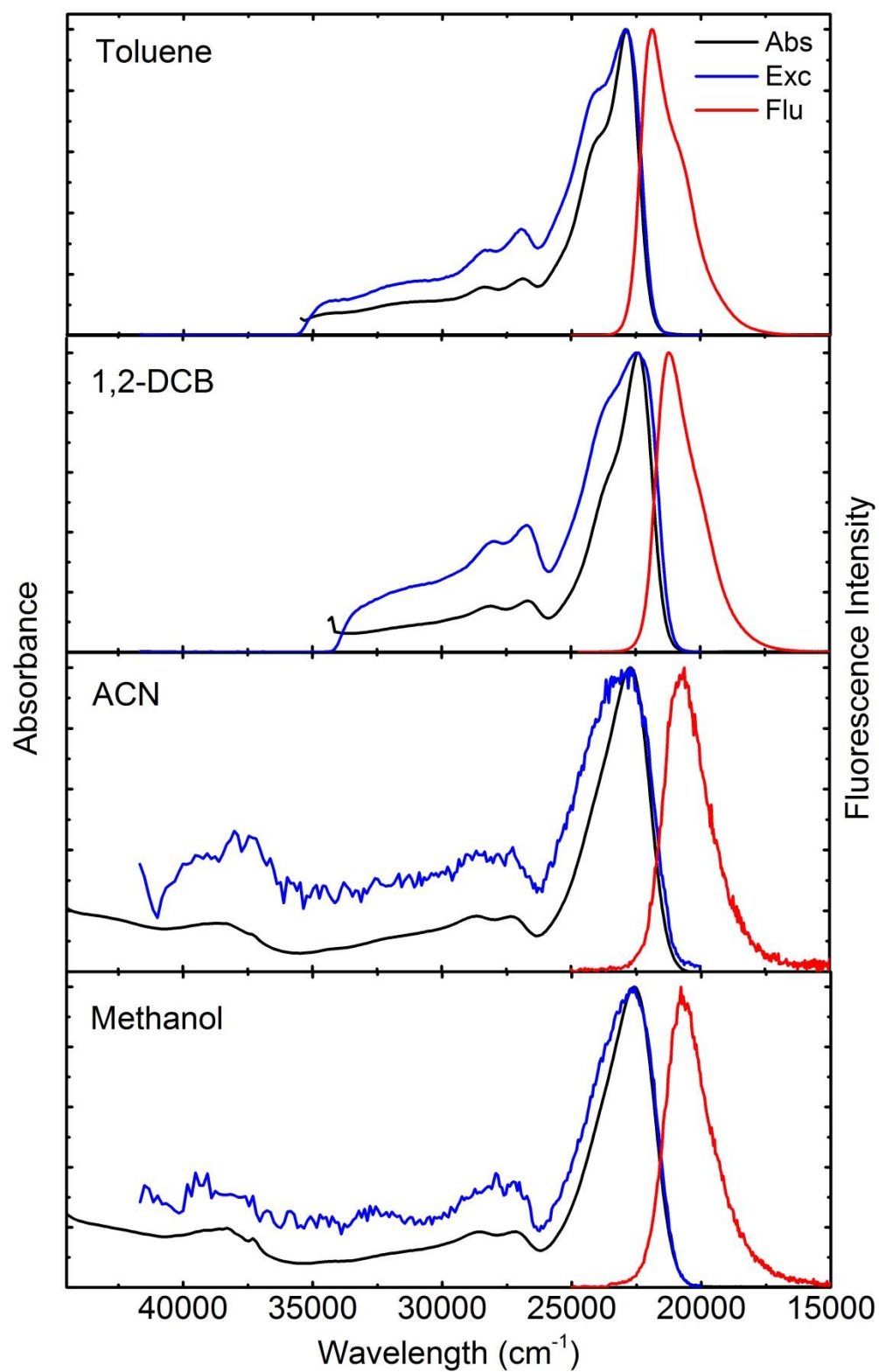


**Figure SF10.** Normalized absorption (black), fluorescence (red) and fluorescence excitation (blue line) spectra of **Amide-7** in toluene, 1,2-dichlorobenzene, acetonitrile and in methanol.

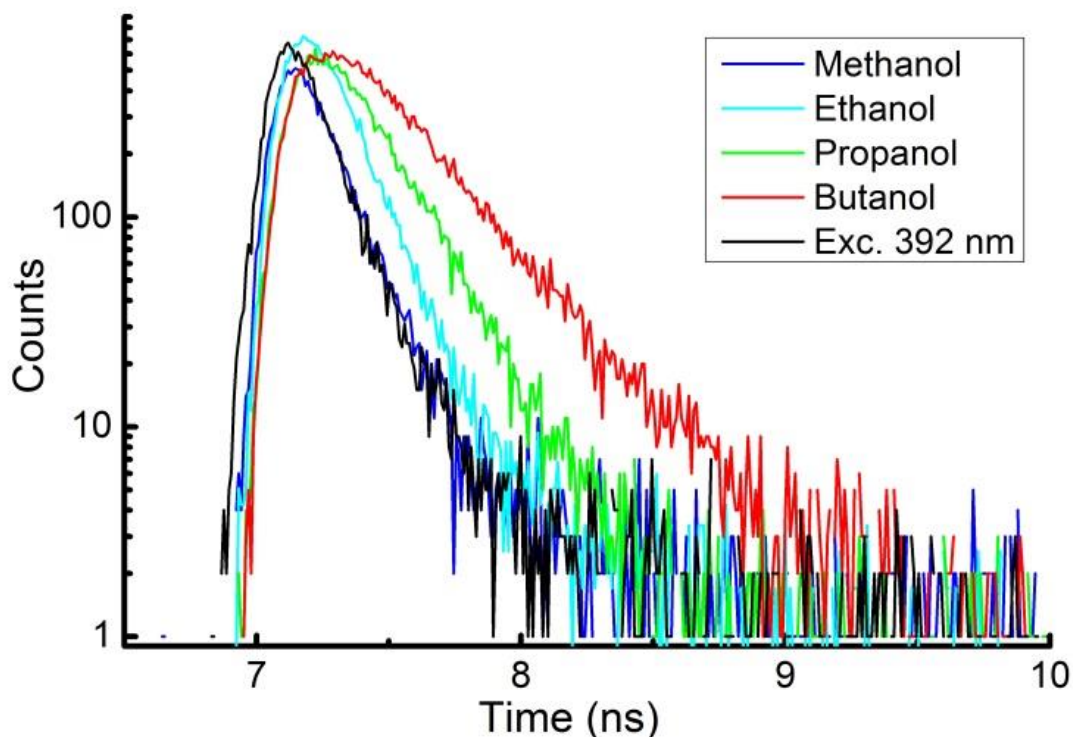


**Figure SF11.** Fluorescence decays of **Amide-7** in methanol, ethanol, propanol and butanol recorded at 480 nm and excitation pulse recorded at 392 nm (black line). Resolution 9.36ps/channel, temperature 21°C.

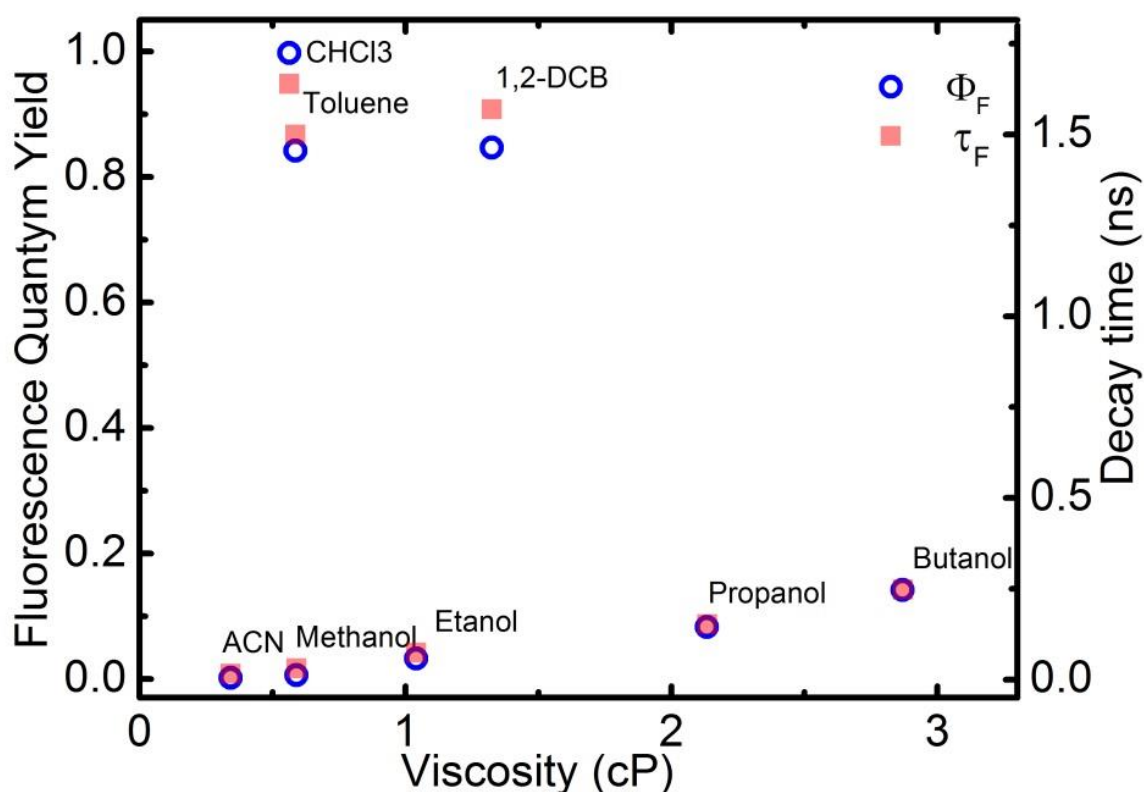


**Figure SF12.** Fluorescence quantum yields ( $\Phi_F$ , blue circles, the left axis) and fluorescence decay times ( $\tau_F$ , red squares, the right axis) of **Amide-7** in selected solvents. Decay times and fluorescence yields change similarly, so the radiative rate  $k_r = \Phi_F / \tau_F$  is constant.

## 6.2 Photophysical Measurements of **Amide-6**

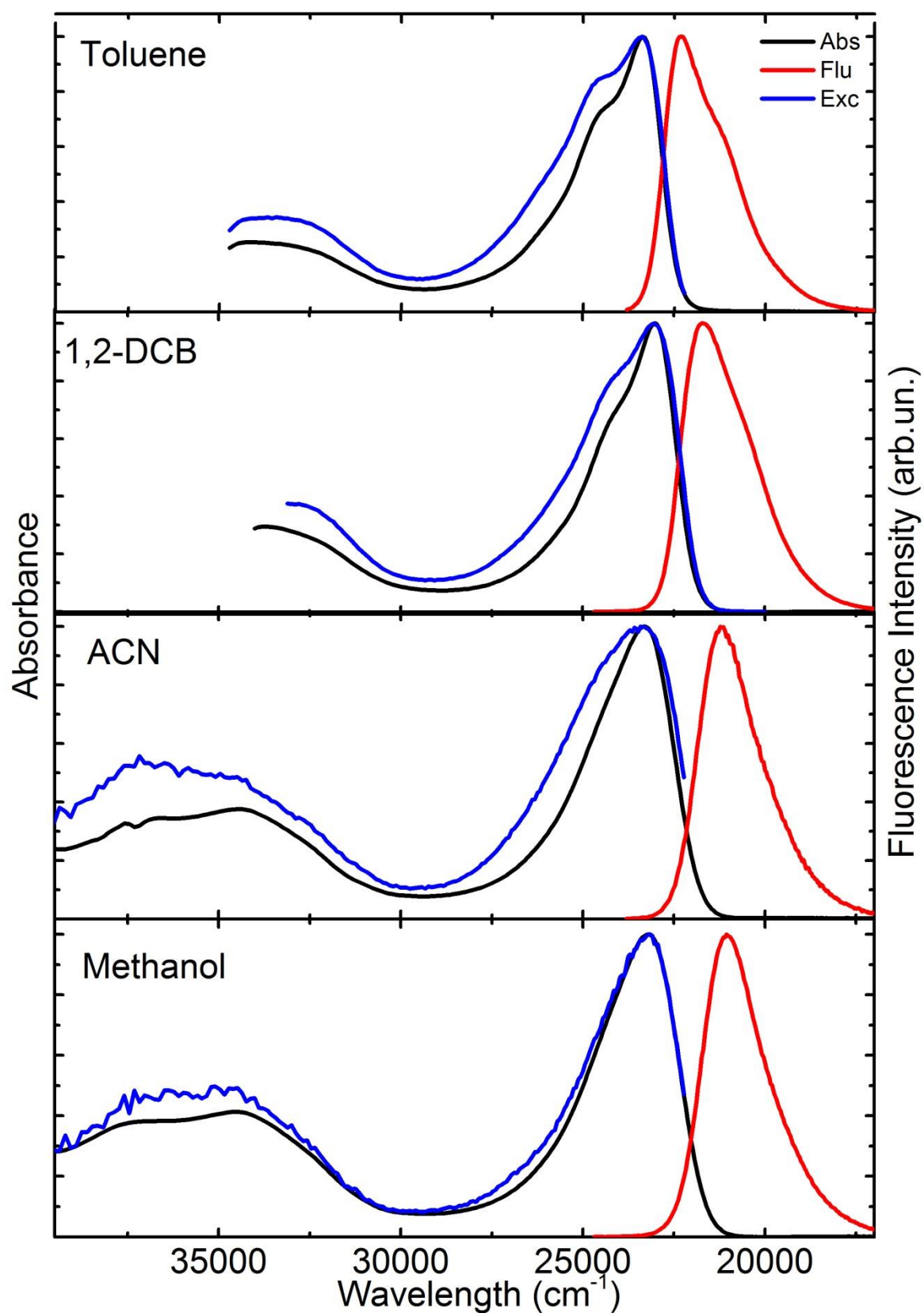


**Figure SF13.** Normalized absorption (black), fluorescence (red) and fluorescence excitation (blue line) spectra of **Amide-6** in toluene, 1,2-dichlorobenzene, acetonitrile and in methanol.



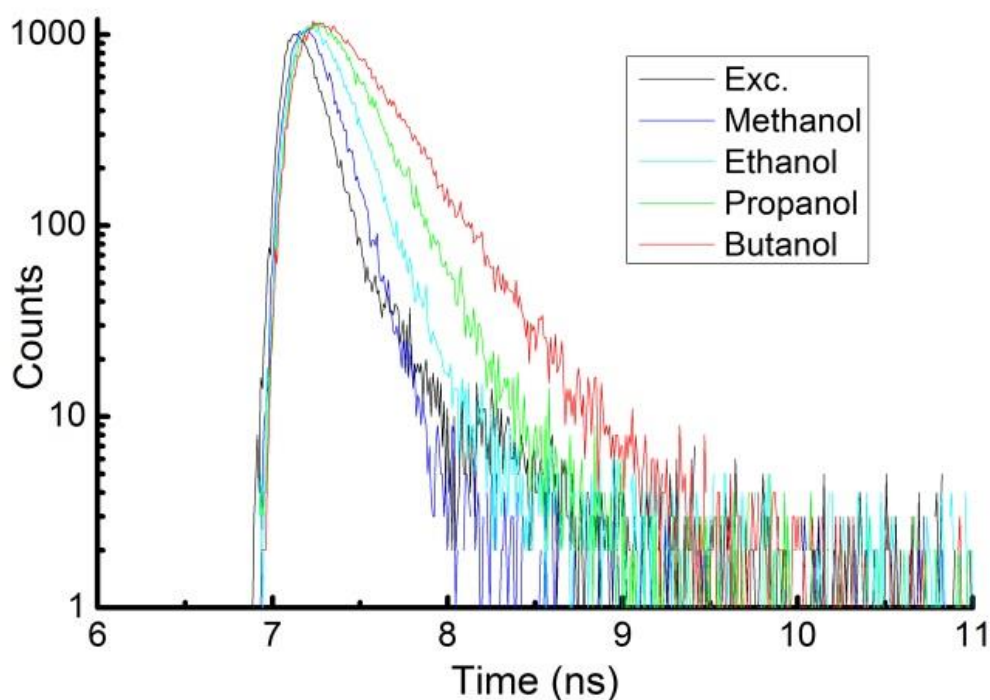


**Figure SF14.** Fluorescence decays of **Amide-6** in methanol, ethanol, propanol and butanol recorded at 480 nm and excitation pulse recorded at 380nm (black line). Resolution 9.36ps/channel, temperature 21<sup>o</sup>C.

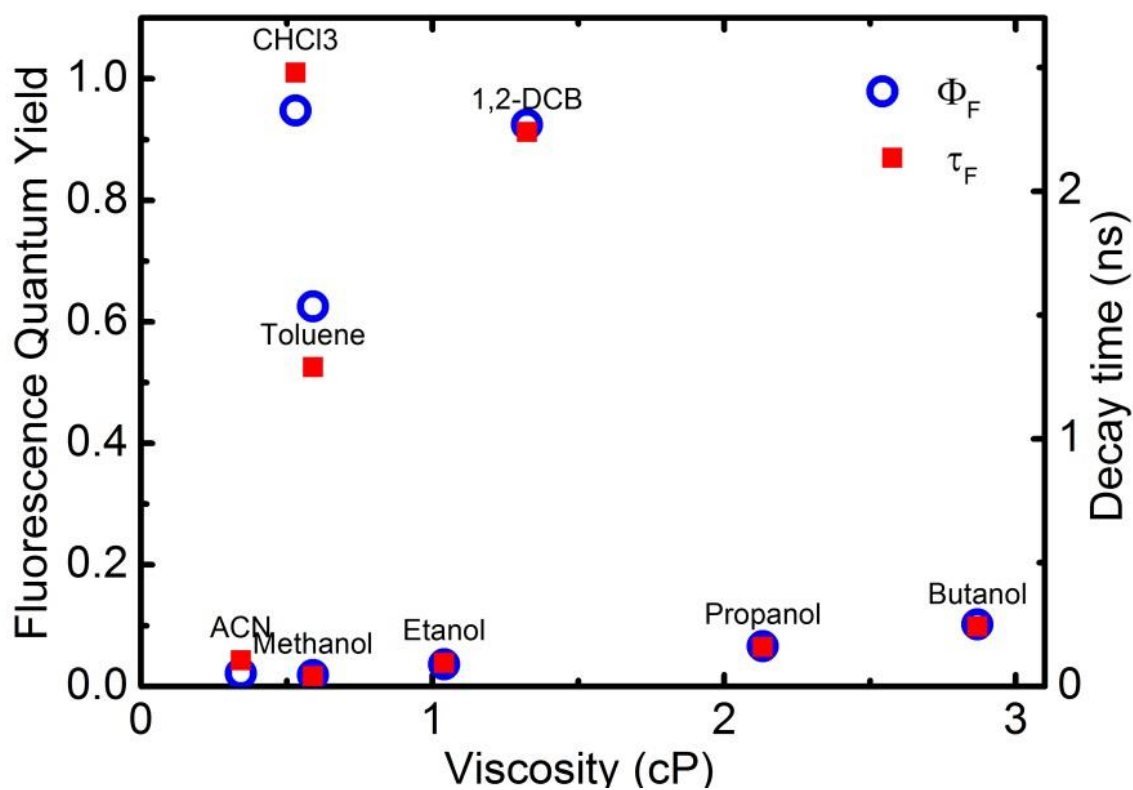


**Figure SF15.** Fluorescence quantum yields ( $\Phi_F$ , blue circles, the left axis) and fluorescence decay times ( $\tau_F$ , red squares, the right axis) of **Amide-6** in selected solvents. Decay times and fluorescence yields behave similarly, so the radiative rate  $k_r = \Phi_F / \tau_F$  is constant.

### 6.3 Photophysical Measurements of **Ester-7**

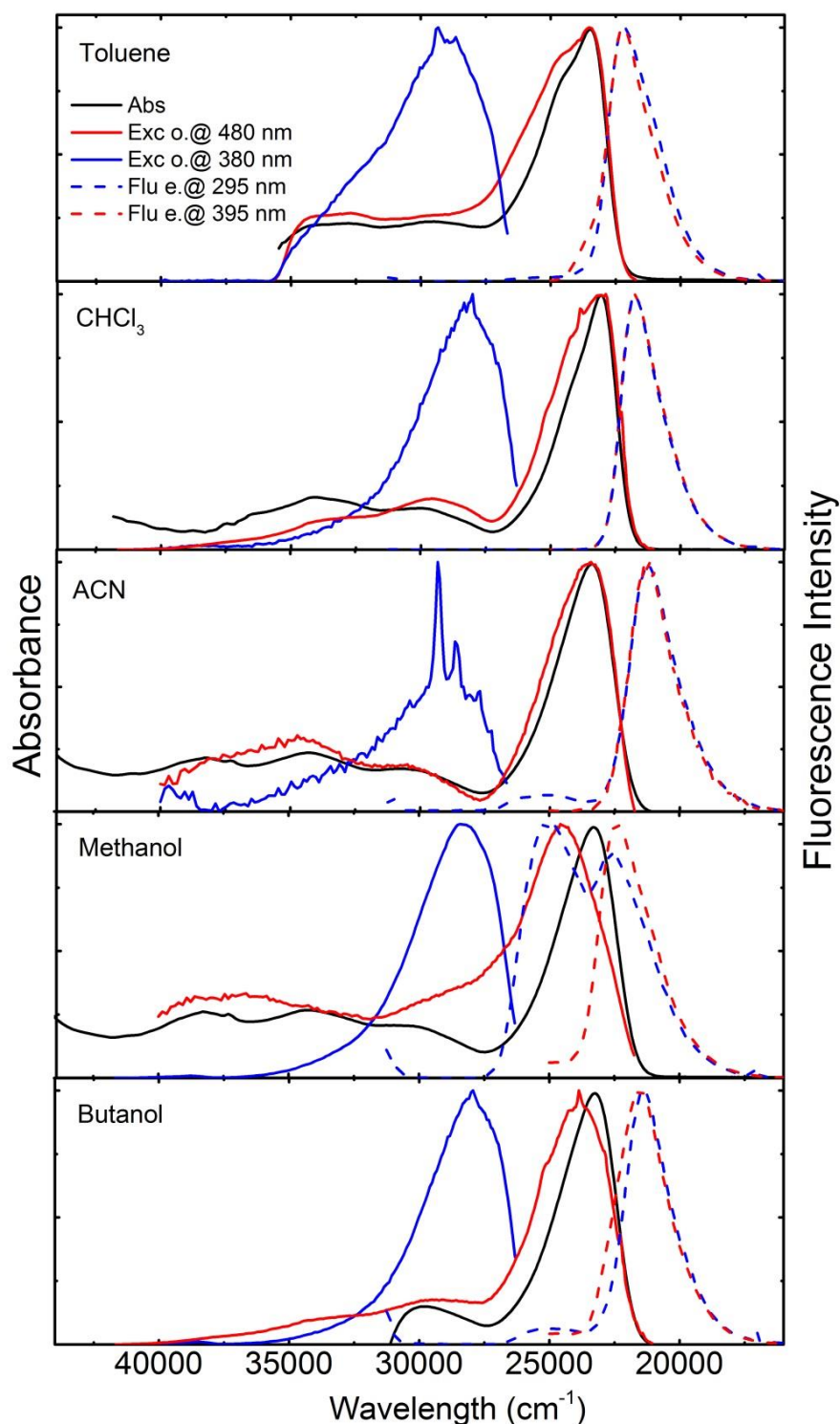


**Figure SF16.** Normalized absorption (black solid lines), fluorescence (dashed lines) and fluorescence excitation (solid lines) spectra of **Ester-7** in toluene,  $\text{CHCl}_3$ , acetonitrile, methanol and in butanol. Blue lines refer to high-energy emissive state (fluorescence spectra excited at 295nm, fluorescence excitation spectra observed at 400nm) whereas red lines refer to the low-energy state (fluorescence spectra excited at 395nm, fluorescence excitation spectra observed at 480nm). The noisy excitation spectrum of **Ester-7** in ACN observed at 400nm (the blue solid line in ACN panel) contains Raman lines of solvent.

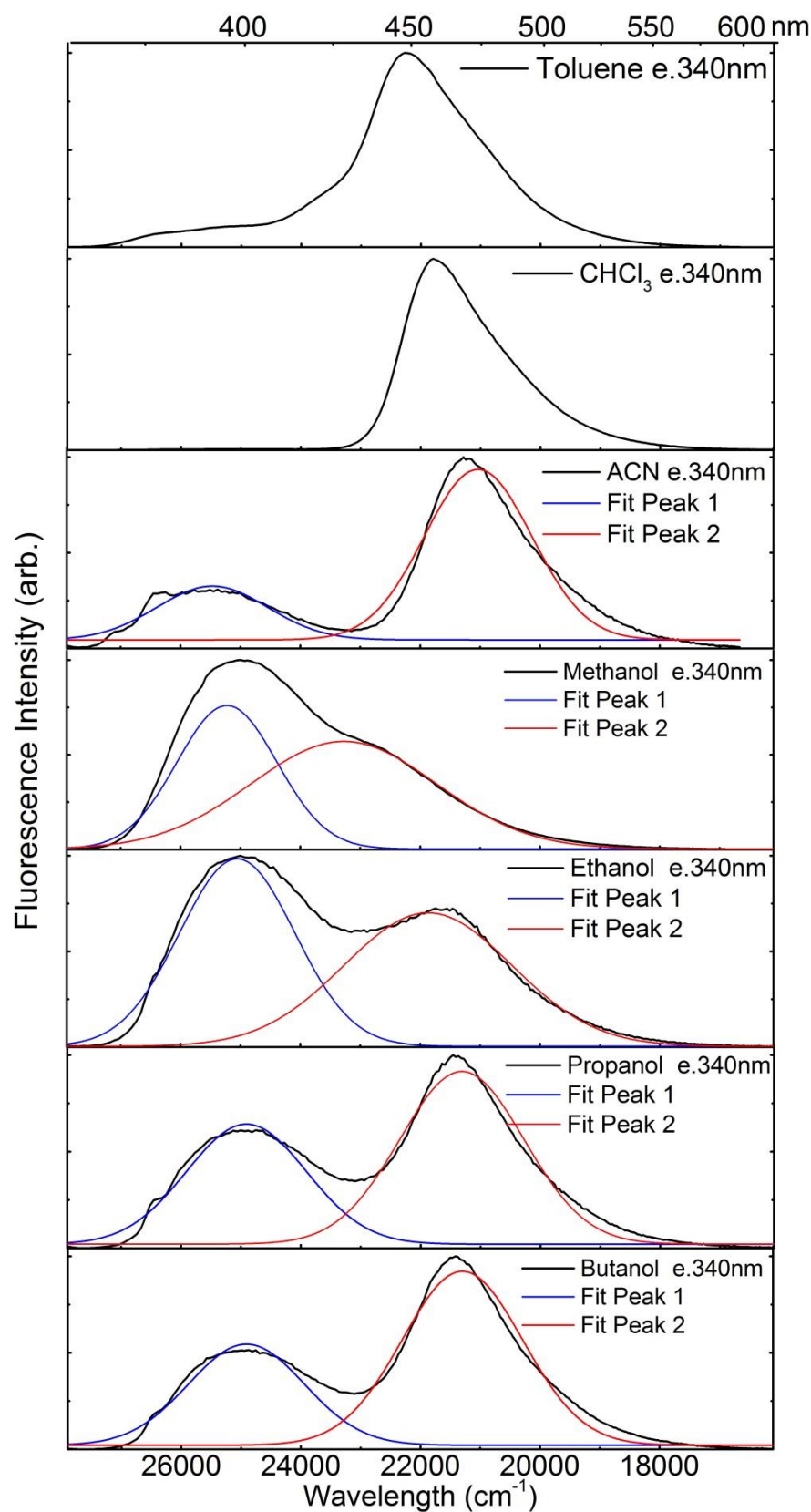


**Figure SF17.** Normalized fluorescence spectra of **Ester-7** in toluene,  $\text{CHCl}_3$ , acetonitrile, methanol, ethanol, propanol and in butanol shown along with the fit of two Gaussian peaks. Blue lines refer to high-energy fluorescence band, red lines refer to the low-energy fluorescence band. Excitation at 340 nm ( $29411\text{cm}^{-1}$ ).



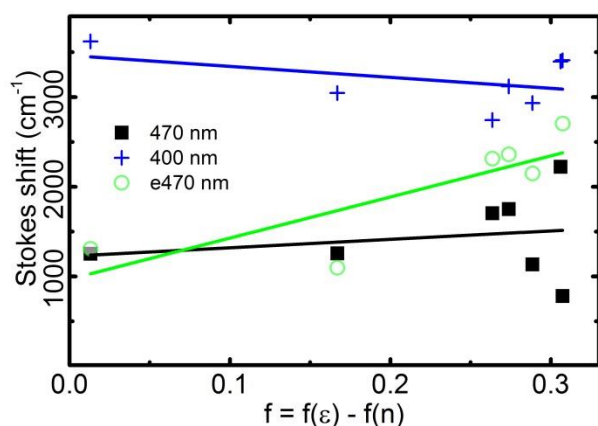


**Figure SF18.** Solvatochromism of optical spectra of **Ester-7** (graphical symbols) and linear fits to experimental points (solid lines). Lippert-Mataga plot of Stokes shifts: black squares - absorption to low-energy fluorescence band (slope  $942 \pm 1949 \text{ cm}^{-1}$ ), green circles - fluorescence excitation to low-energy fluorescence band (slope  $4584 \pm 1377 \text{ cm}^{-1}$ ) and blue crosses - fluorescence excitation to high-energy fluorescence band (slope  $-1220 \pm 1156 \text{ cm}^{-1}$ ).

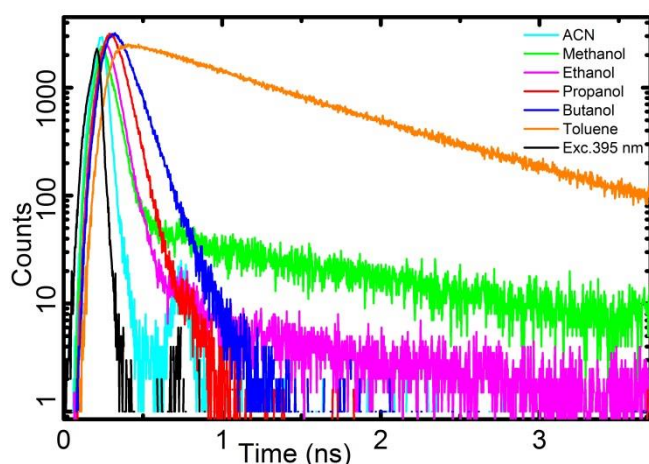


**Figure SF19.** Fluorescence decay profiles of **Ester-7** in selected solvents recorded at 520 nm and excitation pulse recorded at 395 nm (black line). Resolution 2.44ps/channel, temperature  $21^\circ\text{C}$ .

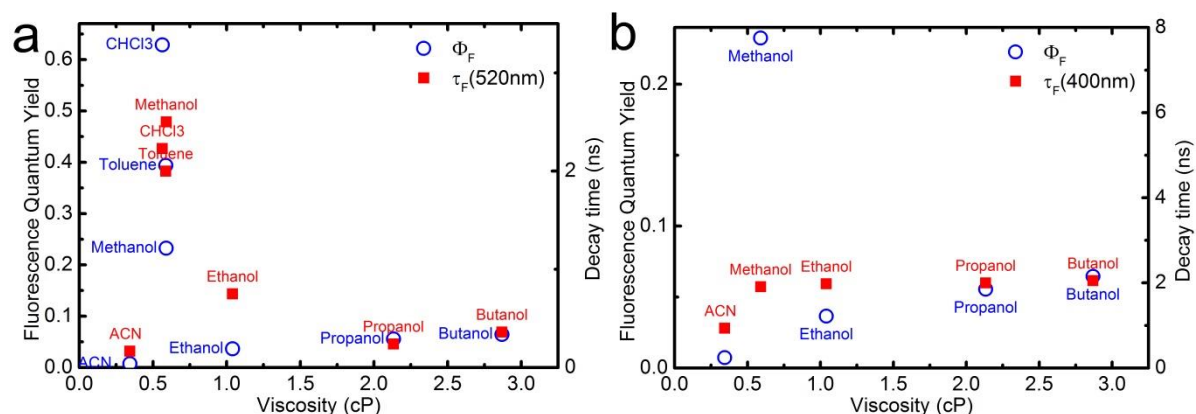


**Figure SF20.** Fluorescence quantum yields (blue circles, the left axis) and fluorescence decay times (red squares, the right axis) of **Ester-7** in solvents. (a) Decay times obtained from decay profiles observed at 520nm with excitation at 336 nm,  $\Phi_F$  obtained from spectra excited at 394 nm (b) decay times from decay curves observed at 400nm with excitation at 336 nm,  $\Phi_F$  obtained from spectra excited at 340 nm.

## 7. IR and Raman spectra

### 7.1 IR and Raman spectra of Amide-7

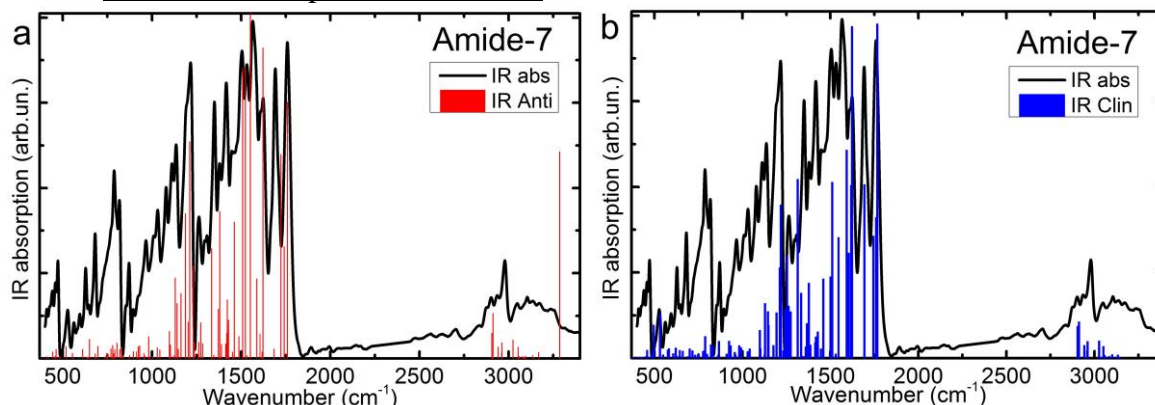


**Figure SF21.** Comparison of IR absorption spectrum of **Amide-7** in KBr pellet (black solid line) with calculated IR spectrum of *Anti* form (a) and *Clin* form (b). IR absorption spectrum taken at room temperature with 4 cm<sup>-1</sup> spectral resolution. Calculated frequencies were multiplied by 0.97 factor.

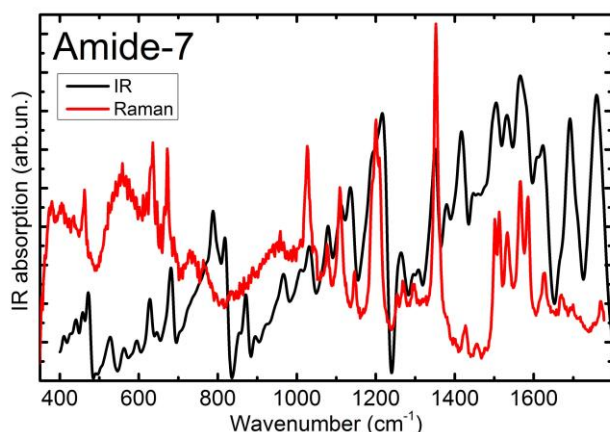


**Figure SF22.** Comparison of IR absorption spectrum of **Amide-7** in KBr pellet (black line) with Raman spectrum of **Amide-7** in powder (red line).

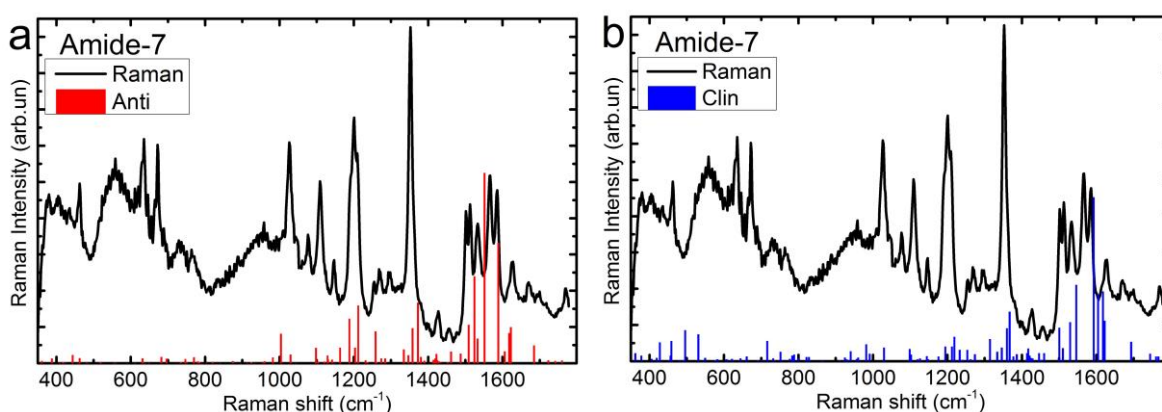


**Figure SF23.** Comparison of Raman spectrum of **Amide-7** in powder (black solid line) with calculated Raman spectrum (vertical bars) of *Anti* form (a) and *Clin* form (b).

At low frequencies, below 1000 cm<sup>-1</sup>, the match between experimental and calculated spectra is weak. For frequencies between 1000 and 1800 cm<sup>-1</sup> the spectra calculated for *Anti* form match better to experimental results.

## 7.2 IR and Raman spectra of **Amide-6**

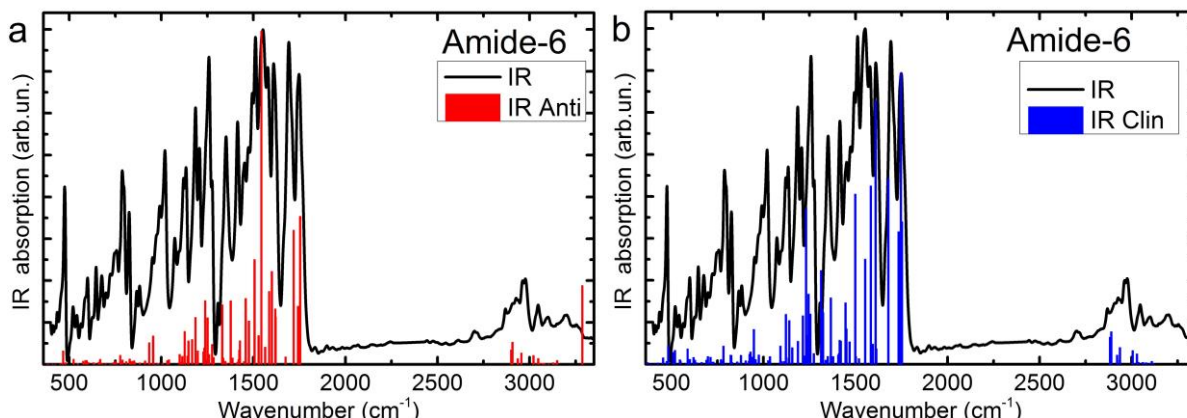


**Figure SF24.** Comparison of IR absorption spectrum of **Amide-6** in KBr pellet (black line) with calculated IR spectrum of *Anti* form (a) and *Clin* form (b). IR absorption spectrum taken at room temperature with 4 cm<sup>-1</sup> spectral resolution. Calculated frequencies were multiplied by 0.97 factor.

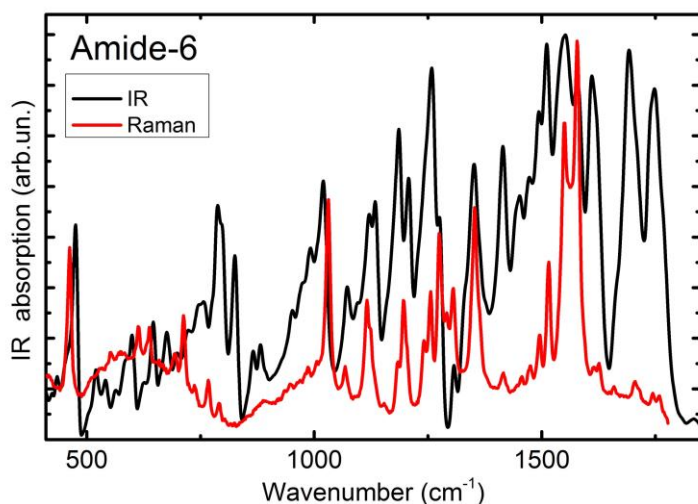


**Figure SF25.** Comparison of IR absorption spectrum of **Amide-6** in KBr pellet (black solid line) with Raman spectrum of **Amide-6** in powder (red solid line).

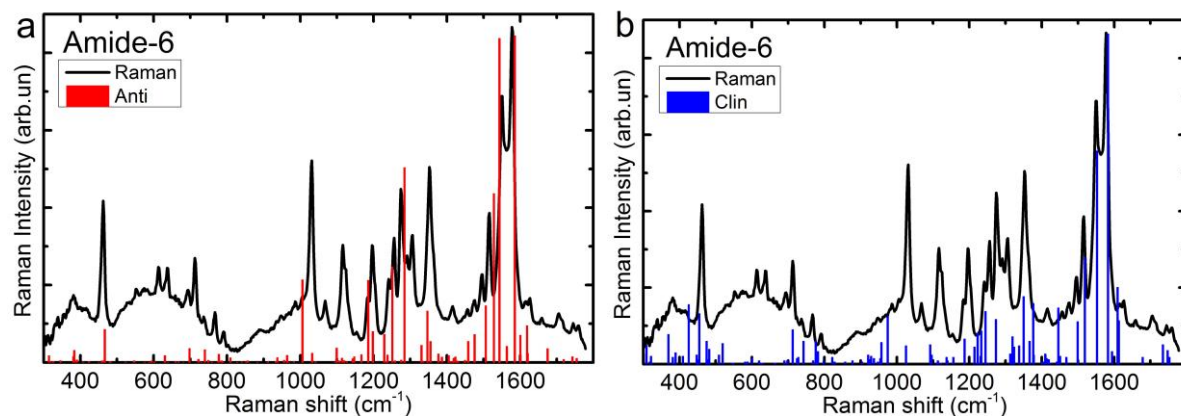


**Figure SF26.** Comparison of Raman spectrum of **Amide-6** in powder (black line) with calculated Raman spectrum (vertical bars) of *Anti* form (a) and *Clin* form (b).

The spectra calculated for *Anti* form match better to experimental results.

### 7.3 IR and Raman spectra of Ester-7

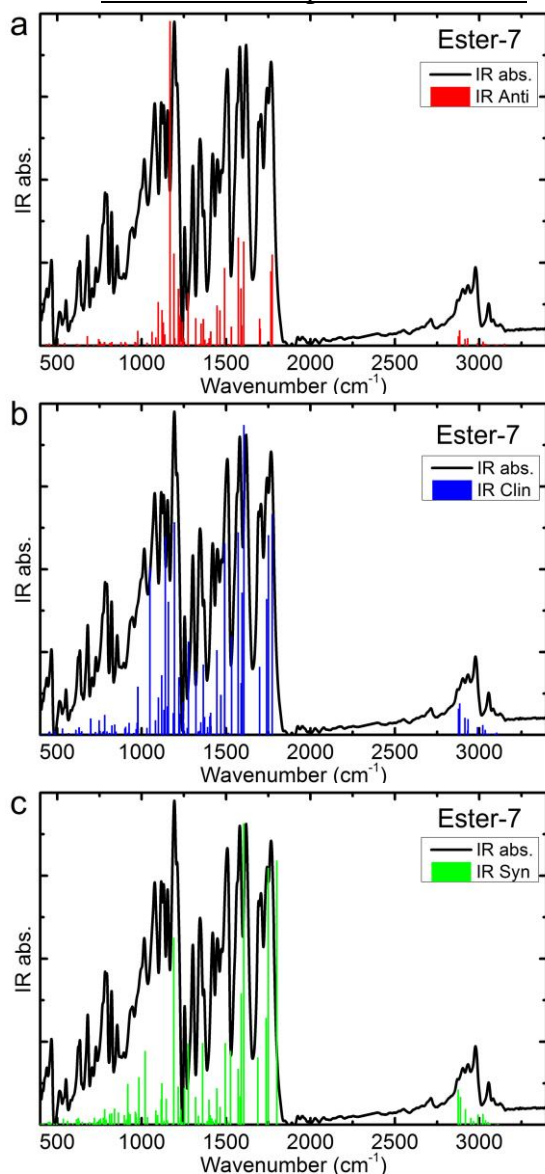


**Figure SF27.** IR absorption spectrum of Ester-7 in KBr pellet (black line) and calculated IR spectrum of *Anti* (a), *Clin* (b) and *Syn* (c) forms.

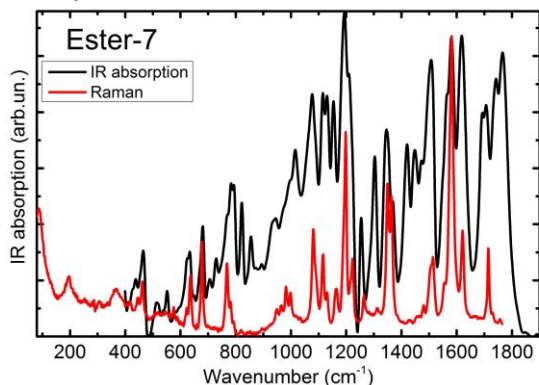


**Figure SF28.** IR absorption and Raman spectra of Ester-7. Raman spectrum of Ester-7 in powder (red solid line).

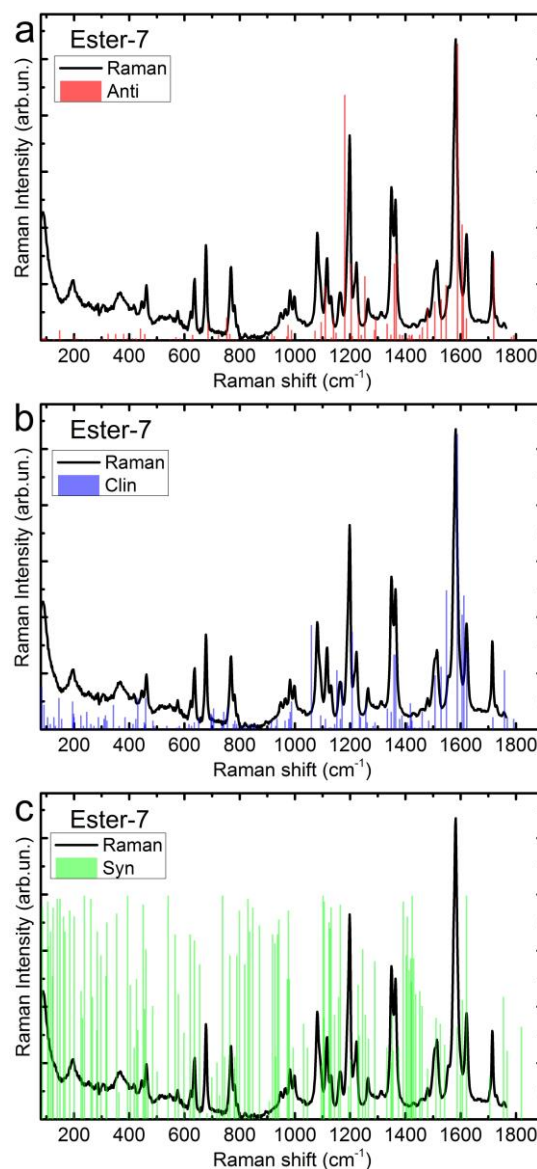


**Figure SF29.** Comparison of Raman spectrum of Ester-7 in powder (black line) with calculated Raman spectrum (vertical bars) of *Anti* form (a), *Clin* form (b) and *Syn* form (c).

IR spectra do not exclude any form. Raman spectra exclude the *Syn* form and point to the presence of two other forms – e.g. *Clin* reproduces well ring CC stretch at  $1582$  and  $1621\text{ cm}^{-1}$  as well as CH bend at  $1080\text{ cm}^{-1}$ , whereas *Anti* fits well to the  $1198\text{ cm}^{-1}$  CH bend.



## 8. Copies of NMR spectra

